Research Square

Preprints are preliminary reports that have not undergone peer review.
They should not be considered conclusive, used to inform clinical practice,
or referenced by the media as validated information.

AI-Driven Modelling and Control of Upper BodyBall and Socket Joints for Enhanced Swimming Performance in Sports Biomechanics

Zeeshan Saeed
Bahria University
Maryam Iqbal
maryamiqbal.buic@bahria.edu.pk

Bahria University
Junaid Imtiaz
Bahria University

Article

Keywords: Biomechanical Model, Sports Biomechanics, Ball and Socket joint, Random Forest, Decision Tree, Linear Quadratic Regulator

Posted Date: May 12th, 2026

DOI: https://doi.org/10.21203/rs.3.rs-7464013/v1

License: This work is licensed under a Creative Commons Attribution 4.0 International License.
Read Full License

Additional Declarations: No competing interests reported.

AI-Driven Modelling and Control of Upper Body Ball-and-Socket Joints for Enhanced Swimming Performance in Sports Biomechanics

Zeeshan Saeed[1], Maryam Iqbal[1*†], Junaid Imtiaz[1†]

[1]Electrical Engineering, Bahria University (BSEAS), H-11, Islamabad, Pakistan.

*Corresponding author(s). E-mail(s): maryamiqbal.buic@bahria.edu.pk;
Contributing authors: zeeshansaeed.h11@bahria.edu.pk;
junaidimtiaz.buic@bahria.edu.pk;
†These authors contributed equally to this work.

Abstract

In front crawl swimming, repetitive upper limb motion imposes substantial mechanical demands on the shoulder joint, potentially reducing performance and increasing injury risk. This study presents a noise aware, simulation based framework that integrates a reduced order biomechanical model, AI based shoulder angle estimation, and classical trajectory tracking control to analyze upper limb coordination under physiologically realistic conditions. This study is positioned as a simulation-based framework focusing on the interaction between prediction uncertainty and control performance. A planar 3 DOF upper limb model, formulated using D'Alembert's principle, is employed to evaluate shoulder abduction dynamics and joint torque profiles. Shoulder abduction angles are estimated from elbow kinematics using Linear Regression (LR), Decision Tree (DT), and Random Forest (RF) models. Although the dataset is synthetically generated, it is constrained within experimentally reported swimming kinematics and validated against literature based range of motion and torque limits. Robustness is assessed by injecting 10% additive Gaussian noise. DT achieves high accuracy in noise free conditions (RMSE ≈ 0.16, $R^2 \approx 0.99$) but degrades under noise, whereas RF demonstrates superior robustness, with a 3 tree ensemble achieving RMSE ≈ 0.34 and $R^2 \approx 0.98$ at low computational cost.

AI predicted shoulder trajectories are directly used as reference inputs for PID and LQR controllers, forming a closed loop pipeline. Results show that prediction uncertainty propagates into control performance, with LQR providing smoother and more accurate tracking than PID, while maintaining joint torques within physiological limits.

Keywords: Biomechanical Model, Sports Biomechanics, Ball and Socket joint, Random Forest, Decision Tree, Linear Quadratic Regulator

1 Introduction

Modern athletes take precautions to improve performance and safety, and biomechanical models simulate human biomechanical models for specific sports to reduce injury risk and maximize technique. Swimming has been on the Olympic calendar since the first modern Olympic Games in 1896 and every summer Olympics after that. Swimming is a beneficial physical and mental activity. Swimming is a popular outdoor sport that improves physical and mental health by allowing the body to move in different postures within the water (Elliott 1999). Swimming helps athletes develop coordination, balance, and core stability, making it a popular cross-training activity.

The human swimming biomechanics model synthesizes swimming motions using numerous frameworks and controllers. Biomechanical human swimming models can be based on four swimming styles: breaststroke, butterfly stroke, backstroke, and crawl (Von Loebbecke et al. 2007). Swimming requires considerable propulsive effort from the upper limbs to drag the body (Pink and Tibone 2000). Upper limbs generate 90% of propulsive force in front crawl swimming (Deschodt et al. 1999) and 88% of swim speed (Pennestri et al. 2007). The upper limb has shoulder, elbow, and wrist joints. The shoulder joint is particularly vulnerable while swimming because it propels the arm movement. Front crawl swimming relies mainly on the hand and forearm (Johnson et al. 2003). The shoulder joint has a broader range of motion than other joints, making it susceptible to injury from repeated arm strokes or technique errors, as given by Lecrivain et al. (2008) and Bedi and Rodeo (2009).

Sports biomechanics aims to reduce injury and boost performance. In research on upper limb biomechanical models in swimming, the author in Lecrivain et al. (2008) created a musculoskeletal model with 24 muscles to assess motions and activations, which emphasizes the significance of upper limb motions and muscular activations in swimming. Expert coaches consider the upper limb the principal velocity generator in swimming, as supported by research Morris et al. (2019). In the research conducted by Lauer et al. (2016), a novel approach was introduced to quantify stresses and moments in the joints of the upper extremities during submerged movements, which can affect training and rehabilitation. A sliding mode controller by the authors in Haghpanah et al. (2023) simulates a front crawl swimmer's upper limb in which elbow and shoulder joints with complete degrees of freedom were modelled. The upper limb biomechanical model was nonlinear. The study by Wang (2024) examines the use of Kinematic Variable Prediction Optimization (KVPO) in sports biomechanics. It showcases the efficiency of KVPO in analyzing and optimizing movement patterns in swimming and

tennis. (Saeed et al. 2025a) developed a three-link physiological motor control model using bond graph analysis and integrated muscle behavior, providing improved insight into musculoskeletal dynamics and neural control. Recent research has advanced artificial muscles by integrating memory and sensory based intelligence, enabling adaptive responses in dynamic environments. These developments, rooted in smart materials and structural innovations, are driving applications in robotics, biomedical devices, and wearable (Oh et al. 2025).

Emerging research highlights the effectiveness of VR and video modelling in enhancing motor skill learning through immersive and visual feedback. This study extends prior work by demonstrating that VR-supported VM significantly improves swimming performance metrics in novices compared to traditional methods (O'sullivan et al. 2022). (Gonzalez et al. 2025) developed biomechanical models of postural control using least squares-based methods to estimate continuous and intermittent feedback parameters, demonstrating adaptive behavior across sensory conditions and age groups and achieving an R^2 of 0.86. The research by (Gračanin et al. 2023) highlights the shoulder joint as the most mobile and injury-prone joint in swimming, emphasizing the importance of strengthening the rotator cuff and scapular stabilizing muscles to reduce injury risk. Similarly, Haghpanah et al. (2023) analyzed swimming-related injuries using a 5-DOF skeletal model with Adaptive Sliding Mode Controllers and identified the shoulder as highly vulnerable during certain phases of the front crawl, estimating an injury risk of about 10

In biomechanical control studies, Iqbal and Roy (2004) applied PID stabilization to a delayed feedback model resembling an inverted pendulum for human posture control, demonstrating effective delay reduction using control-theoretic methods such as the Hermite–Biehler theorem and LMIs, though experimental validation remains necessary. Additionally, Astawa et al. (2023) showed that improved shoulder flexibility and reduced resistance can enhance stroke efficiency and swimming performance, particularly for novice swimmers.

Recent technological approaches also support performance analysis. Hou et al. (2024) developed an intelligent system using genetic algorithms and smartphone video analysis to evaluate swimming techniques with 97.7% accuracy. Furthermore, Voskakis et al. (2024) proposed an underwater arm simulation model in the DAVE virtual environment to study kinematics and hydrodynamic forces. In performance analytics, (Chainok et al. 2023) compared machine learning models for swimming turns and found that the Lasso model performed best for open turns (MSE 0.011, R^2 0.825), while AdaBoost showed better performance for crossover turns, indicating that turn

mechanics significantly affect competitive outcomes.

A light sensor-based image acquisition system was proposed to study swimmer leg movements in Xingyu et al. (2024). This system, which records and analyzes movement, proved more accurate than traditional methods by offering precise water depth measurements and kick off positions, enhancing accuracy. In Bouvet et al. (2024), the authors analyzed intra cyclic and inter cyclic kinematic variability in front crawl swimming. Ninety one swimmers wore sacrum mounted IMU sensors and performed sprints. After preprocessing, a functional double partition model was used to cluster intra-cyclic and inter-cyclic stroke variabilities. These clusters were analyzed for their correlation with swimming speed and performance level using ANOVA, Chi-squared tests, and Gamma statistics. This data-driven approach enhances traditional technical evaluations, providing a valuable tool for optimizing swimming techniques and training strategies. The work (Dos Santos et al. 2024) investigates the shoulder asymmetry torques in competitive swimming. It specifically examines the direction and magnitude of these asymmetries at two different angular velocities, namely 60°/s and 180°/s. The analysis conducted on 21 swimmers enables the measurement of peak torque during internal and external rotation. The main discovery of the study indicated that higher asymmetries are detectable at lower angular velocities, namely 60°/s. This work aims to rectify these imbalances to boost swimming performance, optimize training efficiency, and minimize the likelihood of injuries.

The shoulder complex comprises articulations, osseous structures, muscular tissues, and ligaments, enabling diverse motions. The acromioclavicular, sternoclavicular, scapulothoracic, and coracoclavicular joints are integral components of the musculoplasty. Osteoscopic surgery is a highly effective therapeutic choice for prevalent conditions like impingement, labral tears, and rotator cuff injuries (Funk 2023). Marquina (2025) examines the role of artificial intelligence in personalizing sports training, detailing its applications across multiple disciplines and emphasizing both technological benefits and socio economic disparities in access.

The study reported by (Mononen et al. 2024) highlights the significance of combining artificial intelligence (AI) with biomechanical modelling to enhance the early detection and personalized therapy of osteoarthritis (OA). Implementing machine learning with wearable sensors and Finite Element Analysis (FEA) models could improve the prediction accuracy of AI in predicting the risk and progression of osteoarthritis (OA). The work (Zhao et al. 2024) demonstrates electromyography and motion capture techniques to analyze the kinetics and kinematics of sports biomechanics, aiming for injury prevention and diagnosis. This

approach highlights the use of artificial intelligence (AI) and machine learning (ML) to enhance efficiency by surpassing the constraints of conventional techniques. The work presented by Zhang (2024) utilizes quantum sensors, wearable Internet of Things (IoT) devices, and machine learning (ML) techniques to mitigate abdominal and knee injuries and enhance athletic performance. This is achieved by employing a dual risk classification system that incorporates gaming experience, self-reported injury effects, and postural stability tests in conjunction with ML algorithms. The study presented in Borlaug et al. (2019) investigates the application of sliding mode control (SMC), namely the super twisting algorithm with adaptive gains, for the Underwater Swimming Manipulator (USM) to analyze the most efficient trajectory tracking for a snake shaped robot deployed underwater. The primary aim is to combine thrusters and joints for effective station keeping and trajectory tracking. Demonstrating the highest level of convergence of tracking errors is an essential stage. The subsequent stages involve using a sliding mode observer for state estimation and integrating a second-order sliding mode control (SMC) algorithm. Results from comparative simulations demonstrate that the proposed control law surpasses a linear PD controller in performance. Nevertheless, the study acknowledges certain deficiencies, such as the need to explore control parameters further, expand the findings into three dimensions and practical experiments, and resolve constraints associated with thrusters. A method was developed to estimate instantaneous swimming velocity using a 3-axis inertial measurement unit (IMU). The forward acceleration signal was processed through a drift-free integration algorithm, which included phase-specific filtering and cumulative trapezoidal integration. Positional drift was corrected by constraining the integrated displacement to the known 50 m lap length. This method was validated against a tethered reference system in real world conditions with Paralympic athletes performing all four competitive swimming strokes Clément et al. (2021).

Environmental factors or flaws in the techniques of athletes while swimming can cause a risk of injury and reduce performance. Even though swimming is one of the most played sports worldwide, the scientific study of swimming contributes only about 10 % of the total sports science literature (Costa and Barbosa 2018).

This study investigates upper limb biomechanics in front crawl swimming through a deliberately integrated and focused framework that links biomechanical modelling, data driven inference, and control analysis. Although biomechanical modelling, ML based motion prediction, and classical trajectory tracking controllers have each been widely investigated in swimming biomechanics literature, these components are typically analyzed independently. Limited attention

has been given to understanding how prediction uncertainty from data driven joint angle estimation propagates through biomechanical control pipelines and affects trajectory tracking behaviour under physiologically constrained aquatic motion.

In particular, the study addresses the following research question. *The influence of AI-based shoulder joint-angle prediction uncertainty on closed-loop trajectory tracking performance and joint torque requirements in biomechanically constrained upper-limb swimming motion is investigated.* To address this question, this study develops a simulation-based prediction–control interaction framework that evaluates robustness of shoulder-angle estimation under noise-perturbed sensing conditions, analyzes sensitivity of PID and LQR tracking performance to prediction uncertainty, investigates the influence of anthropometric variability on torque requirements, and provides a physiologically constrained simulation baseline for future wearable sensing integration.

The main contributions of this study are summarized as follows:

- Development of a physiologically constrained simulation biomechanical model of arm linking AI-based shoulder-angle estimation with closed-loop biomechanical trajectory tracking.
- Quantitative evaluation of prediction-error propagation into controller tracking performance and joint torque demand.
- Comparative robustness analysis of PID and LQR controllers using identical AI-generated motion references.
- Sensitivity assessment of lightweight AI prediction performance under noise-perturbed sensing scenarios.
- Establishment of a simulation-based baseline platform supporting future validation with wearable or motion-capture datasets.

The contribution of this work therefore, lies not in proposing a new prediction algorithm or controller, but in establishing a structured framework for analysing the interaction between data-driven motion estimation uncertainty and biomechanical trajectory tracking performance in aquatic upper-limb motion.

The comparative analysis demonstrates that, while classical PID control remains effective, the LQR controller provides superior trajectory smoothness and robustness under noisy conditions. Likewise, although Decision Trees offer computational efficiency, Random Forest models exhibit improved robustness to noise and inter-joint variability. The study, therefore, contributes not by introducing new algorithms but by providing a validated, coherent framework for examining how AI based kinematic inference interacts

with controller design in swimming biomechanics. This integration clarifies the trade-offs between model simplicity, prediction robustness, and control performance, and establishes a foundation for future experimental validation and subject-specific extension.

The hypothesis of the study is aligned as:

1. The integration of AI-based shoulder angle inference with classical linear controllers within a unified biomechanical framework will enable stable and accurate tracking of shoulder abduction trajectories during front crawl swimming, with LQR providing improved smoothness and robustness compared to PID control under noisy conditions.
2. Data-driven joint learning using Decision Tree and Random Forest models can reliably infer shoulder abduction kinematics from elbow motion within physiologically validated bounds, with Random Forest demonstrating greater robustness to noise and variability than a single Decision Tree.

The rest of the paper is structured as follows: we begin with a discussion of the functions and anatomy of the human arm in swimming, followed by modelling of the human arm, dataset generation, and Machine Learning Techniques, i.e., Decision Tree and Random Forest are implemented to predict shoulder trajectory. The model is then simulated with the PID and LQR controllers along with the analyzes. This is followed by a comparison of the performance with the previous study, and the study concludes with the final discussion.

2 Methodology

Modern athletes take precautions to improve performance and safety, and biomechanical models simulate human biomechanics for specific sports to reduce injury risk and maximize technique. Swimming has been on the Olympic calendar since the first modern Olympic Games in 1896 and every summer Olympics after that. Swimming is a beneficial physical and mental activity. Swimming is a popular outdoor sport that improves physical and psychological health. This section outlines the construction of the biomechanical model, the application of control methods such as Linear Quadratic Regulator (LQR) and Proportional Integral Derivative (PID) controllers for managing joint trajectories, and machine learning techniques, including Decision Tree and Random Forest algorithms, for predicting shoulder angles.

2.1 Simulation-based validation of biomechanical models

The study by Nakashima (2009) utilizes the SWUM (SWimming hUman Model) simulation model to analyze humans' extensive range of

motion with their four limbs, in contrast to aquatic creatures with streamlined bodies. The SWUM software enables the determination of swimming speed, body floating, and dynamic movements by solving equations related to rigid body motion. This research aims to enhance the accuracy of fluid force estimations by conducting practical investigations using an underwater robotic arm. Moving forward, the team aims to deepen their understanding of the biomechanical phenomena of human swimming by investigating muscle activation, validating models, and addressing different swimming movements. In the study by Gojkovic et al. (2019), a dynamic model was introduced to capture leg motion in freestyle and backstroke swimming, designed explicitly for rehabilitation following hip and knee surgeries. A Kirchhoff Lagrangian dynamics framework was employed, incorporating a 'robotic swimming leg' model to simplify practical application. The methodology involved developing a comprehensive dynamics model, simulating a user-friendly version, and validating joint angles and muscular torques. The findings emphasized the model's utility for post surgical rehabilitation and its potential application to swimming rehabilitation for amputated individuals, showcasing its clinical relevance and adaptability. Comparative analyzes between simulation platforms (e.g., OpenSim vs AnyBody) demonstrate that consistent joint angle and force predictions can be obtained across validated modelling systems prior to experimental use Gautam et al. (2024). Advances in model augmentation have also shown improved kinematic tracking against marker data in complex upper body movements, supporting the incremental value of enhanced models validated Hu et al. (2025). In addition, domain specific dynamics models for swimming mechanics have been validated through high-fidelity physics simulations such as CFD, indicating the utility of simulation environments for initial validation of motion dynamics Ardister et al. (2025).

2.2 Biomechanical Model of an Upper Limb

This section will discuss modelling the ball, socket, and elbow and wrist joints. Fig. 1 shows the autonomy of the upper limb consisting of the shoulder Gluneuhomeral Joint (Ball and socket joint), the humeroradial elbow joint, and the wrist joint. The glenohumeral joint is responsible for an extensive range of motion, such as abduction and adduction movements. The high range of motion of the shoulder can result in decreased joint stability and can lead to dislocation and injury (Miniato et al. 2023). However, this study's scope focused on shoulder abduction in the sagittal plane a revolute joint approximation was used. This simplification was necessary to make the control analysis tractable and aligns with similar approaches in

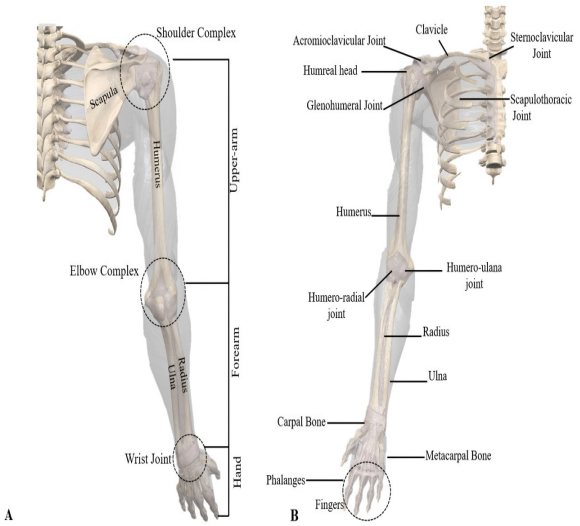


Fig. 1: Anatomy of the upper limb consisting of the shoulder, elbow, and wrist joint (Gull et al. 2020)

biomechanical modelling, where full 3D modelling isn't essential for the variable of interest. In swimming, the upper limb is responsible for producing the required propulsive force to move the body in the forward direction. The glenohumeral joint is responsible for producing maximum propulsion force along with the elbow and hand, which directly face the drag force of water. In this study, a mathematical model of an upper limb from the Superior or frontal axis is modelled, considering the upper trunk and whole body as a rigid body and the shoulder, elbow, and wrist joints as movable joints. This modelling uses shoulder abduction/ adduction, elbow flexion/ extension, and wrist flexion in freestyle swimming.

Recent literature confirms that using reduced-order, planar models focusing on primary motions (such as shoulder abduction, elbow flexion, and wrist movement) is a justified and common approach when the research objective is to analyze task-specific kinematics or control behavior rather than reproduce the full physiological complexity of the upper limb. A scoping review of shoulder joint modelling using OpenSim notes that many upper limb simulations rely on idealized inputs and simplified representations that do not reflect all in-vivo physiological conditions, yet remain widely used for kinematic and dynamic investigations of specific motions such as abduction or flexion due to their computational tractability and clarity of interpretation Fonseca et al. (2025). Similarly, recent modelling studies compare simplified modelling assumptions in software platforms and demonstrate substantial differences in muscle force predictions and dynamics when full musculoskeletal complexity is considered, emphasizing that simplified DOFs are purposeful modelling choices rather than oversights Gautam et al. (2024). Study on personalized 3D shoulder and elbow models shows that increasing anatomical fidelity (e.g., subject-specific joint centers) improves kinematic accuracy but also substantially raises complexity, which may exceed the scope of studies targeting control or pattern differences in specific planar tasks such as swimming abduction movements

Hammond et al. (2025). A study conducted by (Ichikawa et al. 2006) use two segments modelling of the upper limb, having fore arm and upper limb, to demonstrate the movement of the elbow and shoulder without considering all aspects of the shoulder joint.

System identification and joint/muscle stiffness studies show that simplified models can capture the dominant dynamics relevant for torque estimation and control, without modelling full muscle-tendon or hydrodynamics explicitly Cop et al. (2021). These studies either simplify, partially consider, or do not explicitly formulate full hydrodynamic force models Zaidi et al. (2008), Sayahkarajy and Witte (2025),
Takagi et al. (2016). The study modelled a human hand impaired model using Bond graph without modelling of musculoskeletal dynamics Iqbal et al. (2013). Phase-specific biomechanical analyzes often use simplified representations to estimate torque stability and muscle coordination during task-specific motions, supporting the validity of reduced-order models for controlled movement studies Li et al. (2025). The study proposes a fuzzy logic–based cascade control strategy for coordinated motion of the ring and little fingers using a bio-mechanical model, but it does not incorporate detailed muscle–tendon dynamics in the system modelling Iqbal and Rasool (2025). The study modelled a bio-mechanical hand with joint motions without modelling of musculoskelal dynamics Saeed et al. (2025b). While the present 3-DOF model does not explicitly include muscle-tendon dynamics or hydrodynamic forces, simplified planar and reduced-order upper-limb models are widely used in biomechanics and control studies to capture dominant motion dynamics and joint torques. This approach ensures computational tractability for AI-based prediction and controller evaluation, while preserving physiologically meaningful insights.

2.3 D'Alembert's Law

The total of all forces acting on a body equals zero according to D'Alembert's principle as given in (Talamucci 2024). This expression modifies Newton's Law equation to incorporate a negative sign before the product of mass and acceleration; this law claims that the sum of the force (F) and this altered component (-ma) equals zero: F - ma = 0. This law implies that the object reaches a state of equilibrium when exposed to both the actual force (F) and a hypothetical force (-ma). For the rotational systems, this law becomes:

$$\sum \tau = 0 \tag{1}$$

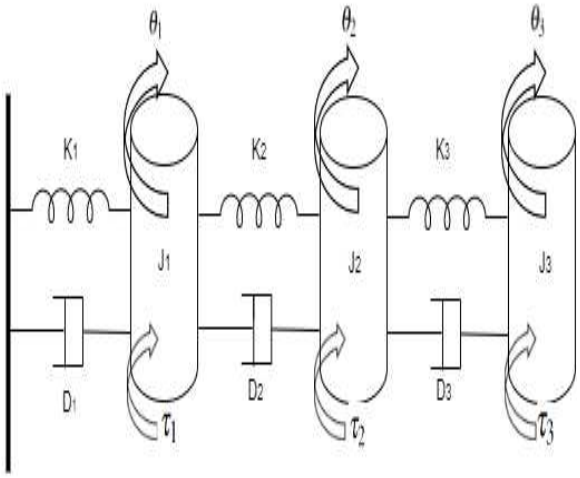


Fig. 2: Schematic representation of the biomechanics of the upper limb

2.4 Mathematical Equations for a 3-DOF Upper Limb Model

The mathematical modelling of the theoretical mechanical system is based on D'Alembert's Law. Fig. 2 represents the linear mathematical model diagram for arm motion with 3-DOF for shoulder, elbow, and wrist joints. The model is formed using Newton's law of motion for rotating bodies.

The model also considers the angle of rotation (θ), damping (D), stiffness (K), and moment of inertia (J) components of each joint.

Rotational Displacements:

- θ_1 : Rotational displacement at the shoulder joint
- θ_2 : Rotational displacement at the elbow joint
- θ_3 : Rotational displacement at the wrist joint

Stiffness Coefficients:

- K_1: Stiffness coefficient for the shoulder joint
- K_2: Stiffness coefficient for the elbow joint
- K_3: Stiffness coefficient for the wrist joint

Damping Coefficients:

- D_1: Damping coefficient for the shoulder joint
- D_2: Damping coefficient for the elbow joint
- D_3: Damping coefficient for the wrist joint

Input Torque:

- τ_1 : Rotational displacement at the shoulder joint
- τ_2 : Rotational displacement at the elbow joint
- τ_3 : Rotational displacement at the wrist joint

The state space equation of the resulting sixth-order model is given as follows:

$$\dot{\vec{x}}(t) = A\vec{x}(t) + B\vec{u}(t), \tag{2}$$

Here, $\vec{x}(t)$represents the physiologically relevant states of the biomechanical model, $\vec{u}(t)$

represents the input control supplied by the compensator to emulate the action of the Central Nervous System (CNS).

The following equation represents the state vector:

$$\overrightarrow{x}(t) = [\theta_1, \theta_2, \theta_3, \omega_1, \omega_2, \omega_3]^T \tag{3}$$

Matrix $A \in \mathbb{R}^{6\times6}$ is the state matrix governing the dynamics of the six states inherent to the model. $B \in \mathbb{R}^{6\times1}$ denotes the single input, representing the muscle force applied to the model's shoulder joint. $C \in \mathbb{R}^{1\times6}$ represents an output matrix and $D \in \mathbb{R}^{1\times1}$ represents a zero matrix.

$$A = \begin{bmatrix} 0 & 0 & 0 & 1 & 0 & 0 \\ 0 & 0 & 0 & 0 & 1 & 0 \\ 0 & 0 & 0 & 0 & 0 & 1 \\ -\frac{K_1+K_2}{J_1} & \frac{K_2}{J_1} & 0 & -\frac{D_1+D_2}{J_1} & -\frac{D_2}{J_1} & 0 \\ \frac{K_2}{J_1} & -\frac{K_2+K_3}{J_2} & \frac{K_3}{J_2} & \frac{D_2}{J_2} & -\frac{D_2+D_3}{J_2} & \frac{D_3}{J_2} \\ 0 & \frac{K_3}{J_3} & -\frac{K_3}{J_3} & 0 & \frac{D_3}{J_3} & -\frac{D_3}{J_3} \end{bmatrix} \tag{4}$$

$$B = \begin{bmatrix} 0 \\ 0 \\ 0 \\ \frac{1}{J_1} \\ \frac{1}{J_2} \\ \frac{1}{J_3} \end{bmatrix} \tag{5}$$

$$C = \begin{bmatrix} 1 & 0 & 0 & 0 & 0 & 0 \end{bmatrix} \tag{6}$$

$$D = \begin{bmatrix} 0 \end{bmatrix} \tag{7}$$

The overall system, including measured and regulated variables, is given as follows:

$$\begin{bmatrix} \dot{\theta}_1 \\ \dot{\theta}_2 \\ \dot{\theta}_3 \\ \dot{\omega}_1 \\ \dot{\omega}_2 \\ \dot{\omega}_3 \end{bmatrix} = \begin{bmatrix} 0 & 0 & 0 & 1 & 0 & 0 \\ 0 & 0 & 0 & 0 & 1 & 0 \\ 0 & 0 & 0 & 0 & 0 & 1 \\ -\frac{K_1+K_2}{J_1} & \frac{K_2}{J_1} & 0 & -\frac{D_1+D_2}{J_1} & -\frac{D_2}{J_1} & 0 \\ \frac{K_2}{J_2} & -\frac{K_2+K_3}{J_2} & \frac{K_3}{J_2} & \frac{D_2}{J_2} & -\frac{D_2+D_3}{J_2} & \frac{D_3}{J_2} \\ 0 & \frac{K_3}{J_3} & -\frac{K_3}{J_3} & 0 & \frac{D_3}{J_3} & -\frac{D_3}{J_3} \end{bmatrix} \begin{bmatrix} \theta_1 \\ \theta_2 \\ \theta_3 \\ \omega_1 \\ \omega_2 \\ \omega_3 \end{bmatrix} + \begin{bmatrix} 0 \\ 0 \\ 0 \\ \frac{1}{J_1} \\ \frac{1}{J_2} \\ \frac{1}{J_3} \end{bmatrix} u(t) \tag{8}$$

$$y(t) = \begin{bmatrix} 1 & 0 & 0 & 0 & 0 & 0 \end{bmatrix} \begin{bmatrix} \theta_1 \\ \theta_2 \\ \theta_3 \\ \omega_1 \\ \omega_2 \\ \omega_3 \end{bmatrix} + \begin{bmatrix} 0 \end{bmatrix} u(t) \tag{9}$$

The numerical values of the different physiological parameters of the natural human hand are given in Table 1 & Table 2 respectively as discussed below:

Table 1 shows the length and weight of each limb of a human arm.

Table 1: Human Arm Segment Weight and Length as Percentage of Body Weight and Height ExRx.net (2019)

Limb	**Proximal**	**Distal**	**Weight (% of w)**	**Length (% of h)**
Forearm	Shoulder	Elbow	3.25%	17.2%
Elbow	Elbow	Wrist	1.87%	15.5%
Hand	Wrist	Fingertip	0.65%	5.75%

The length (l) and weight (w) of the limb for a person of body weight (B_w= 65Kg and height (B_h)= 1.625m by using the following equations:

$$W_s = \frac{W \times 3.25}{100} \tag{10}$$

$$W_e = \frac{W \times 1.87}{100} \tag{11}$$

$$W_h = \frac{W \times 0.65}{100} \tag{12}$$

$$L_s = \frac{L \times 17.2}{100} \tag{13}$$

$$L_e = \frac{L \times 15.7}{100} \tag{14}$$

$$L_h = \frac{L \times 5.75}{100} \tag{15}$$

The moment of inertia (J) is calculated for the limb of mass (m), and the length (l) is calculated by

$$J = m \cdot l^2 \tag{16}$$

Table 2 shows the parameters (D and K) that are adopted from literature (Gielen and Houk 1984; Xu and Hollerbach 1999; Formica et al. 2012; Huber et al. 2019) and used in Equation 8.

Table 2: Human Hand Physiological Parameters

Joints	J **(kg · m^2)**	D **(N · m · s/rad)**	K **(N · m/rad)**
Shoulder	0.1650	1	15
Elbow	0.0771	2	30
Wrist	0.0037	0.03	3

2.5 Dataset Acquisition and Joint Trajectory Estimation

In this study, a dataset of upper-limb joint kinematics is constructed to support feasibility analysis of AI-based joint angle prediction and control in front-crawl swimming. The dataset is not obtained from direct experimental measurements; instead, it is generated using experimentally validated joint motion models reported in prior swimming biomechanics literature.

Specifically, Ichikawa et al. (2003) experimentally estimated shoulder and elbow joint angles during the front crawl technique using synchronized accelerometer and video-based measurements. In that study, the underwater motion of the arm was modelled using two rigid segments, namely the upper arm and the forearm. The elbow joint was modelled as a revolute joint allowing flexion and extension, while the shoulder joint motion was represented by its dominant abduction movement during the underwater propulsion phase. Following this experimentally established

framework, the present study defines the shoulder abduction angle (θ_{SA}) and elbow flexion angle (θ_{EF}).

The joint angle trajectories are generated using mathematical formulations originally introduced and validated using experimental swimming data and shown to reproduce the temporal evolution of upper-limb joint motion during front crawl swimming Ichikawa et al. (2006). The shoulder abduction and elbow flexion angles are estimated using Eq. (17) and Eq. (18).

$$\theta_{\mathrm{SA}} = \theta_{\mathrm{SA,max}}\, e^{-k_{\mathrm{SA}}(t-t_{\mathrm{SA,max}})^2} \tag{17}$$

$$\theta_{\mathrm{EF}} = \theta_{\mathrm{EF,max}}\, e^{-k_{\mathrm{EF}}(t-t_{\mathrm{EF,max}})^2} \tag{18}$$

The parameter values used in this study are adopted from experimentally validated swimming studies. Specifically, the maximum shoulder abduction and elbow flexion angles are set to $\theta_{\mathrm{SA,max}} = 10^\circ$ and $\theta_{\mathrm{EF,max}} = 180^\circ$, respectively, while the corresponding peak times are chosen as $t_{\mathrm{SA,max}} = 1.25\,\mathrm{s}$ and $t_{\mathrm{EF,max}} = 1.0\,\mathrm{s}$. The shaping parameters are selected as $k_{\mathrm{SA}} = 18.62$ and $k_{\mathrm{EF}} = 16.8$, which provide good agreement with experimentally measured joint trajectories.

The trajectories are computed for a swimmer with a time interval ranging from $t = 0$ to $t = 2$ seconds. To incorporate age-related performance variation, a decline of 0.6% per year reported in swimming performance studies Rubin et al. (2013) is considered. Therefore, by using Eq. (19), Eq. (20), and Eq. (21), variations in the swimmer's performance are estimated.

$$\text{max_time_after_}x\text{_years} = \frac{\text{initial_max_time}}{(1-\text{annual_reduction_rate})^{\text{years}}} \tag{19}$$

$$\text{max_angle_after_}x\text{_years} = \frac{\text{initial_max_angle}}{(1-\text{annual_reduction_rate})^{\text{years}}} \tag{20}$$

$$\text{K_parameters_after_}x\text{_years} = \frac{\text{initial_K_parameter_value}}{(1-\text{annual_reduction_rate})^{\text{years}}} \tag{21}$$

where annual_reduction_rate = 0.6% and years = 25.

The dataset consists of approximately 800 samples, generated using parametric joint trajectory models. The age range (25–43 years) is incorporated to introduce variability; however, the dataset does not represent a statistically validated population distribution. The assumption of a 0.6% annual performance decline is used as a simplified approximation and may not be uniformly applicable across swimmers of different skill levels.

It should be noted that data cannot fully capture physiological and environmental factors such as muscle activation dynamics, soft tissue deformation, and hydrodynamic interactions present in real swimming motion.

2.6 Dataset Input–Output Correlation Analysis

A correlation study was conducted on a dataset consisting of three input variables, i.e., age, time, and elbow joint angle, and the output shoulder abduction angle, in order to determine whether the chosen input features contribute to trivial learning behavior. The goal of this analysis is to measure the degree to which the shoulder trajectory may be linearly encoded by any one input variable, which could otherwise simplify the learning problem to a simple temporal or parametric mapping.

Table 3 provides a summary of the Pearson correlation coefficients calculated for the training and testing datasets. The findings show that, with correlation values near zero, age and time have very little linear association with the shoulder abduction angle. This demonstrates that the shoulder trajectory is not only determined by age or time but also provides contextual and temporal structure to the learning problem. In the training dataset, there is a slight inverse relationship between elbow joint angle and time. The non-monotonic, Gaussian-shaped joint trajectories are the source of this behavior, which is not indicative of deterministic temporal encoding.

The elbow joint angle shows a moderate relationship with shoulder abduction, indicating inter joint connection that is bio mechanically significant. However, when taken into account separately, this correlation is insufficient for reliable inference because elbow motion alone cannot capture subject specific variability or temporal evolution of the movement. Therefore, the model's capacity to generalize across subjects and precisely recreate joint coordination in noisy and age factor affecting performance would be diminished if age and time were excluded.

Table 3: Pearson Correlation Analysis Between Input Variables and Shoulder Abduction Angle in the dataset

Variable	**Training Data**	**Testing Data**	**strength**
Age vs θ_{SA}	0.030	–	Negligible
Time vs θ_{SA}	0.017	0.292	Weak
θ_{EF} vs θ_{SA}	0.413	0.393	Moderate
Time vs θ_{EF}	-0.170	0.007	Weak

These results demonstrate that the learning task necessitates the integration of temporal information, subject-specific characteristics, and inter-joint dynamics rather than being reduced to a single input mapping. As shown in later control tracking investigations, this multi variable formulation is crucial for attaining strong AI based prediction and guaranteeing dependable downstream control performance.

2.7 AI Models for Predicting Shoulder Angle

While Deep learning (DL) architectures like LSTMs and CNNs provide high predictive capacity, they are often hindered by high computational costs and high execution times Justus et al. (2018). In trajectory prediction specifically, these resource-heavy models face significant challenges regarding multi-factor feature extraction and real time feasibility Jiang et al. (2025). Since the dataset used in this study is simulation-constrained and relatively low-dimensional, ensemble-based methods provide an appropriate balance between prediction robustness, interpretability, and computational efficiency for evaluating prediction control interaction effects.

Three regression based AI models are used in this study to predict the shoulder abduction angle during swimming: Random Forest (RF), Decision Tree (DT), and Linear Regression (LR). From straightforward linear relationships to nonlinear ensemble learning techniques, these models reflect various degrees of model complexity. Their capacity to deduce the shoulder joint angle from biomechanical input factors like elbow angle and temporal stroke characteristics is to be assessed.

Linear Regression (LR): Because of its ease of use and interpretability, linear regression is utilized as a baseline prediction model. The predicted shoulder angle $\theta_s(t)$ and the input feature vector $\mathbf{u}(t)$ are assumed to have a linear relationship. The expression for the LR model is James et al. (2023).

$$\hat{\theta}_s(t) = \mathbf{w}^\top \mathbf{u}(t) + b \tag{22}$$

where $\hat{\theta}_s(t)$ denotes the predicted shoulder angle at time t, $\mathbf{u}(t)$ represents the input feature vector, $\mathbf{w}$ is the regression coefficient vector, and b is the bias term. where $\hat{\theta}_s(t)$ denotes the predicted shoulder angle at time t, $\mathbf{u}(t)$ represents the input feature vector, $\mathbf{w}$ is the regression coefficient vector, and b is the bias term.

Decision Tree (DT): Decision Tree regression is a non-parametric learning method that predicts target variables by recursively partitioning the feature space into decision regions. DT models are capable of capturing nonlinear relationships between biomechanical variables and joint motion while remaining computationally efficient and interpretable Rokach and Maimon (2005).

Random Forest (RF): Random Forest is an ensemble learning technique that improves prediction accuracy by combining the outputs of multiple decision trees constructed using random subsets of training data and features. The final prediction is obtained by averaging the outputs of all trees in the ensemble. RF models are particularly effective for biomechanical

datasets with nonlinear patterns and variability Behjati Ashtiani et al. (2024).

These models have been widely applied in biomechanics and medical movement analysis for predicting joint behavior and identifying abnormal motion patterns Prodanovic et al. (2024). In this study, their performance is evaluated in terms of prediction accuracy for estimating the shoulder abduction angle from the available kinematic inputs.

2.8 Gaussian Noise Injection and Output Smoothing

In upper limb biomechanical modelling, measurement uncertainty arises from sensor noise, soft tissue artifacts, and modelling inaccuracies Poitras et al. (2019). To emulate these uncertainties and evaluate model robustness, Gaussian noise was injected into the synthetic kinematic dataset. This approach is commonly used when experimental motion data are unavailable and provides a practical approximation of measurement errors in IMU and motion capture systems (Gabela et al. 2019; Bishop and Nasrabadi 2006). Many signal processing and control frameworks, particularly Kalman filtering, assume measurement noise to be Gaussian due to its mathematical tractability and ability to approximate aggregate random disturbances via the central limit theorem. This assumption enables efficient estimation and has been widely validated in multi-sensor and biomechanical systems, where Gaussian noise is often used as a first order approximation of sensor uncertainty Gunawardane et al. (2021). Additionally, constant-variance Gaussian noise models are commonly adopted to represent baseline sensor noise characteristics in filtering and simulation studies Chhabra et al. (2021). Therefore, Gaussian noise provides a reasonable and widely accepted baseline for initial validation before incorporating more complex, real-world noise effects.

Machine learning models trained on noise-free data often show overly optimistic performance and may not generalize well to real sensing conditions. Therefore, additive Gaussian noise was introduced into both the input features and the output joint angle references during training Gonzalez (2009); Goodfellow et al. (2016):

$$\tilde{\mathbf{X}}_{\text{train}} = \mathbf{X}_{\text{train}} + \boldsymbol{\eta}_X, \quad \tilde{\mathbf{y}}_{\text{train}} = \mathbf{y}_{\text{train}} + \eta_y, \tag{23}$$

$$\boldsymbol{\eta}_X \sim \mathcal{N}(\mathbf{0}, \sigma_X^2 \mathbf{I}), \quad \eta_y \sim \mathcal{N}(0, \sigma_y^2), \tag{24}$$

where the noise magnitudes are scaled relative to the variability of the signals:

$$\sigma_X = \alpha \cdot \mathrm{std}(\mathbf{X}_{\mathrm{train}}), \quad \sigma_y = \beta \cdot \mathrm{std}(\mathbf{y}_{\mathrm{train}}). \quad (25)$$

Following the approach of (Jeon and Lee 2024), a moderate noise level of $\alpha = \beta = 0.1$ (10%) was used to approximate realistic sensor disturbances. This formulation represents measurement uncertainty rather than physiological variability and enables systematic evaluation of model robustness under practical sensing conditions Fantozzi et al. (2016).

To reduce high-frequency fluctuations in predicted joint angles caused by noisy training data, a one-dimensional Gaussian smoothing filter was applied to the predicted output Gonzalez (2009):

$$\hat{y}_{\mathrm{smooth}}(t) = \sum_{\tau} \hat{y}(\tau)\, G(t-\tau), \quad (26)$$

$$G(k) = \frac{1}{\sqrt{2\pi}\sigma_g} \exp\Big(-\frac{k^2}{2\sigma_g^2}\Big), \quad (27)$$

where $\sigma_g = 2$ controls the degree of smoothing. This filtering reduces prediction jitter while preserving the overall joint trajectory, producing signals suitable for biomechanical analysis and control applications Bishop and Nasrabadi (2006); Goodfellow (2016).

2.9 Evaluation Parameters

The R^2 method is the most commonly used evaluation method for regression-trained models. It ranges from 0 to 1 (Breiman 2001). The model that best fits the data will have a score near 1. If all the predicted and actual values are the same, the R^2 will have a score of 1; similarly, a poor model will have a score near 0, while lower or negative values indicate poor explanatory power

$$SSr = \sum_{\substack{k=1 \\ k=n}} (Zi^* - Zi_{(avg)})^2 \quad (28)$$

where Zi^* is the estimated value, and $Zi_{(avg)}$ is the average value of the predicted dataset.

$$SSt = \sum_{\substack{k=1 \\ k=n}} (Zi - Zi_{(avg)})^2 \quad (29)$$

where Zi is the actual value and $Zi_{(avg)}$ the average value of the predicted dataset.

$$R^2 = 1 - \frac{SSres}{SStot} \quad (30)$$

where R^2 is R-squared.

Another evaluation method for the regression model is the Root Mean Squared Error (RMSE). It is the difference between actual and machine learning predictive results. It shows how well a model performed in Wang and Lu (2018), gives an analysis of the use of RMSE in evaluating the performance of the model, and the RMSE formula is given by:

$$\mathrm{RMSE} = \sqrt{\frac{1}{N}\sum_{i=1}^{N}(y_i - \hat{y}_i)^2} \quad (31)$$

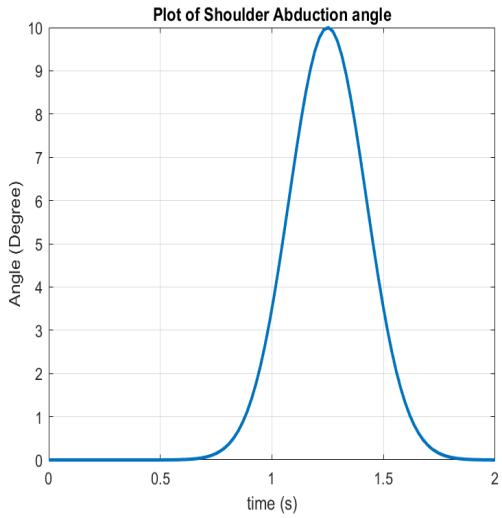


Fig. 3: Shoulder angle trajectory for one swimming cycle in degrees

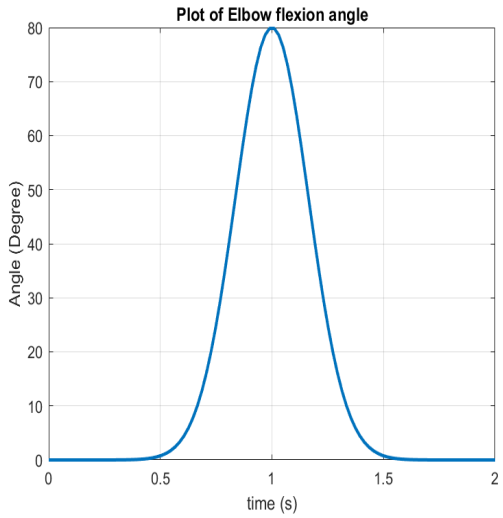


Fig. 4: Elbow angle trajectory for one swimming cycle in degrees

Where:

N : Number of observations

y_i : Actual value for observation i

$\hat{y}_i$: Predicted value for observation i

The lower the RMSE value, the better the model predicts results; it basically shows the error ratio of predicted results.

3 Simulation

Equations 17 and 18 are used to generate the trajectory of the shoulder's abduction angle (θ_{SA}) and elbow's flexion angle (θ_{EF}). They are estimated for a person for one complete swimming cycle.

Fig. 3 & 4 are used to generate the dataset.

The desired trajectory is for one person by using Equation 19, 20, and 21. The parameters are changed as per the age of a person from 25 to 43 years, with a difference of 3 years.

Fig. 5 & 6 shoulder abduction angle (θ_{SA}) and elbow flexion angle (θ_{EF}) trajectories for different swimmers with ages from 25 to 43 years) for time duration t = 0 to 2.5 sec with an interval of 0.01 sec. For testing, a person aged 26 years is used for testing AI models, whose angle trajectories are shown in Fig. 7. (Ichikawa et al. 2006) estimated the time for hand entry and exit in to the water for at t = 0.25s the arm enters in the water is referred as "stroke enter phase" and remains in the water till t= 1.8s which is referred as "stroke phase" where arm exist the water which is refer

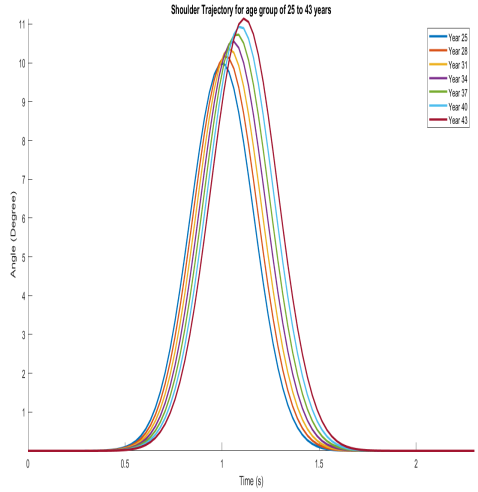


Fig. 5: Dataset representation for multiple people Shoulder Abduction angle trajectory for one complete swimming cycle in degrees

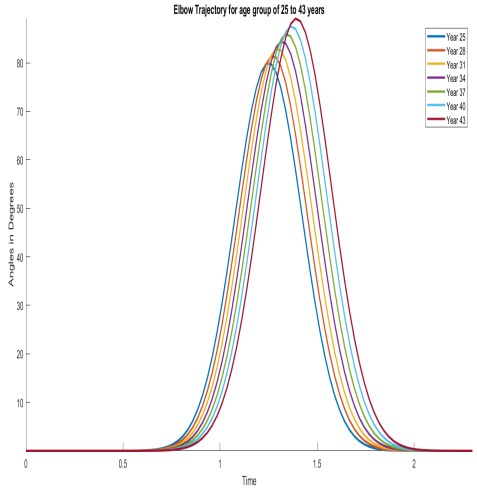


Fig. 6: Dataset representation for multiple people's elbow flexion angle trajectory for one complete swimming cycle in degrees

as "exist phase" and t= 2.2s the arm ready for re-entry in the water.

3.1 Elbow–Shoulder Kinematic Coupling for Data-Driven Estimation

Wearable inertial sensing studies consistently report that shoulder joint angle estimation is more challenging and less reliable than elbow angle estimation due to the shoulder's multi-DoF nature and sensitivity to sensor placement and soft tissue artifacts. El-Gohary and McNames (2012) demonstrated that accurate shoulder angle tracking using IMUs requires complex kinematic modelling and multiple sensors, whereas elbow joint angles exhibit lower estimation error and higher repeatability under comparable sensing conditions. A systematic review by Carnevale et al. (2019) further highlighted that shoulder kinematics show greater variability and methodological inconsistency across wearable sensor studies compared to more distal joints, emphasizing the difficulty of robust shoulder motion estimation in ecological settings. Poitras et al. (2019) reported increased estimation errors for shoulder angles during complex and multi-planar movements, even when validated IMU systems were employed.

A recent systematic review and meta-analysis of upper extremity IMU validity reported that while inertial sensors can measure range of motion reasonably well overall, their performance diminishes for complex multi-plane movements and

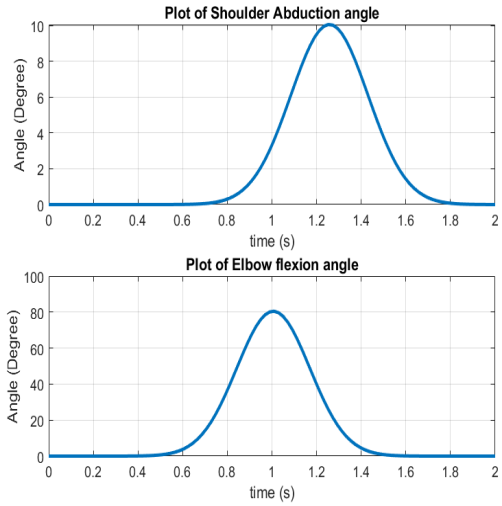


Fig. 7: Shoulder abduction and Elbow flexion angle trajectory for testing of AI model

specific joints such as the shoulder, where accuracy and validity were notably lower than for some simpler joint estimations, suggesting the need for careful algorithm design and improved sensor fusion strategies to achieve reliable shoulder kinematics measurement Li et al. (2024). Another focused review on quantifying shoulder motion in free-living environments emphasized the limited options for IMU placement and fixation that minimize soft tissue effects, and the significant challenges in developing algorithms that produce accurate shoulder joint angles from acceleration and angular velocity data alone, which further underscores the difficulty of direct shoulder angle estimation in wearable contexts Cain and Morrow (2025).

The literature supports the notion that shoulder kinematics estimation via wearable IMUs is inherently less robust and more sensitive to placement, calibration, and motion complexity than joint estimation for anatomically simpler segments like the elbow, thereby motivating the use of elbow-based surrogate estimation as a more reliable input for control systems under constrained sensing conditions.

3.2 Simulation and Results of Artificial Intelligence (AI) Models

The generated synthetic dataset is used to train and evaluate the proposed AI models within a simulation-based framework. The input features include age, normalized time within the swimming stroke cycle, and elbow joint angle, while the shoulder abduction angle is considered the target output. Although the dataset is generated using deterministic parametric formulations, the time variable captures a significant portion of the trajectory structure.

Three classical machine learning models—Linear Regression (LR), Decision Tree (DT), and Random Forest (RF)—are employed due to their interpretability and suitability for small to moderate datasets. All training and testing are performed using synthetic data; therefore,

the reported results represent methodological performance rather than real-world guarantees.

Fig. 8 illustrates the workflow used for shoulder angle prediction. The dataset is divided into training and testing sets and used to train LR, DT, and RF models. For the RF model, different numbers of trees (2, 3, 25, and 100) are used to analyze the effect of model complexity on prediction accuracy.

Model performance is evaluated under three scenarios: (i) noise-free conditions, (ii) Gaussian noise added to both input and output signals, and (iii) Gaussian smoothing applied to predicted outputs to reflect biomechanical signal behavior. In each case, predicted shoulder angle trajectories are compared with reference values over time. Performance is assessed using the coefficient of determination (R^2) and Root Mean Square Error (RMSE), and the results are summarized in a table to compare the robustness and accuracy of each AI model across scenarios.

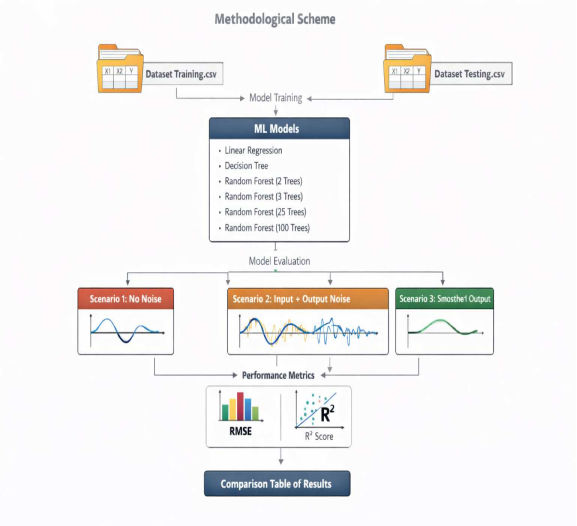


Fig. 8: Methodology scheme for AI Models

3.3 Scenario 1 (No Noise) :

Fig. 9 and Table 4 show the simulation results of expected shoulder abduction paths under the no noise condition. Stroke enter phase at t= 0.25s and stroke exist phase after t= 1.8s the predicted results for all AI models shown no error except for LR, during stroke phase the variation in results can be observed the DT model closely follows the reference path during the whole stroke phase, as the dataset is clean and predictable. DT works very well in this case, with an RMSE score of 0.16 and R^2 0.99. This is because the tree can learn exact threshold-based mappings between the input and output variables. This perfection can also be a result of its property of overfitting.

Random Forest (RF) models also perform very well with the reference trajectory, but for small group sizes, their predictions are a little less accurate and smoother than DT's. The RF performance steadily gets better as the number of trees grows, as when trees are 100, it shows an RMSE value of 0.19, close to DT. This shows that ensemble learning improves the ability to approximate even when conditions are perfect. Linear Regression (LR), on the other hand, doesn't take into account the shape of the trajectory, so it makes a prediction that is too smooth and skewed, which

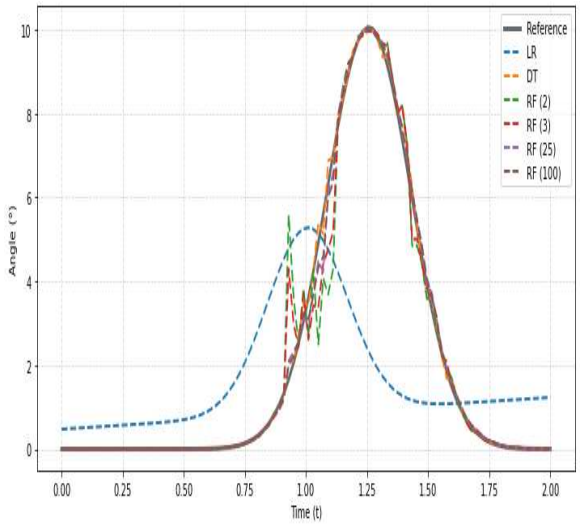


Fig. 9: Predicted shoulder abduction trajectories under noise-free conditions. The reference trajectory (black) is compared with predictions obtained using Linear Regression (LR), blue; Decision Tree (DT), orange; and Random Forest (RF) models with 2 (green), 3 (red), 25 (purple), and 100 (brown) trees.

is much smaller than the peak angle. This proves that the connection between arm movement, time, and shoulder abduction is naturally not linear and cannot be shown in a straight line.

Table 4: Evaluation results for Scenario 1: No Noise

Model	Time (s)	RMSE value	R^2 value
LR	0.001801	2.9762	0.1722
DT	0.009120	0.1627	0.9975
RF (2)	0.018366	0.6725	0.9577
RF (3)	0.029163	0.4743	0.9790
RF (25)	0.166490	0.2049	0.9961
RF (100)	0.806518	0.1905	0.9966

Fig. 10 shows the output angles and the actual angles for the no noise scenario. The ideal prediction line (y=x) is shown by the black diagonal line, where there is perfect agreement between the ground truth and the forecast. Particularly at low and mid range angles, the Linear Regression (LR) model clearly shows a nonlinear departure, indicating underfitting and an incapacity to capture complicated interactions. Although flexibility is increased by the Decision Tree (DT), there is still a discernible scatter from the optimum line. As the number of estimators rises, Random Forest (RF) models show increasingly better alignment with the ideal line. The tightest grouping around y=x is seen in RF with 25 and 100 trees, suggesting higher accuracy and lower variation. This demonstrates how ensembles enhance generalization.

3.4 Scenario 2: Input and Output Noise

Fig. 11 illustrates the predicted shoulder abduction trajectories when Gaussian noise is added to both the input features and the output shoulder angle. This scenario represents a realistic experimental condition in which uncertainty exists not only in elbow joint measurements but also in shoulder angle estimation, as commonly reported in IMU based biomechanical studies due to sensor

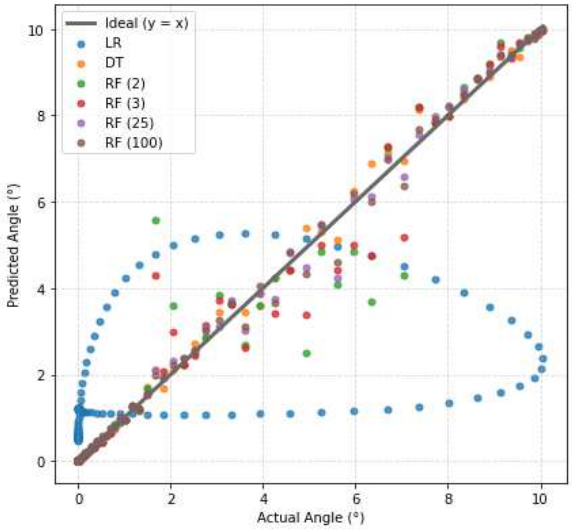


Fig. 10: Actual versus predicted angles for Scenario 1.

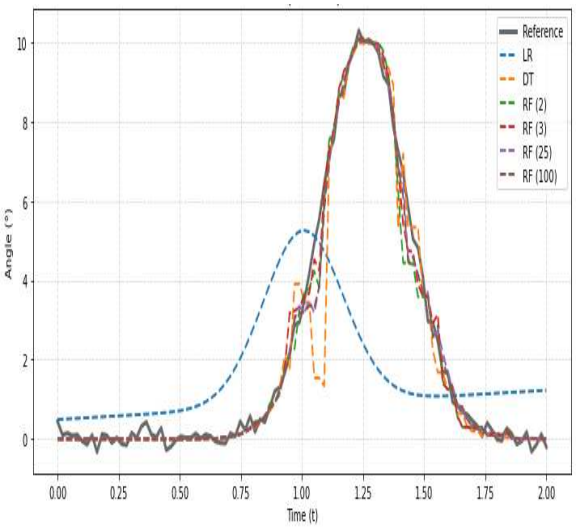


Fig. 11: Predicted shoulder abduction trajectories under Gaussian noise. The reference trajectory (black) is compared with predictions obtained using Linear Regression (LR, blue), Decision Tree (DT, orange), and Random Forest (RF) models with 2 (green), 3 (red), 25 (purple), and 100 (brown) trees.

misalignment, soft tissue artifacts, and multi-DOF shoulder motion.

Table 5: Evaluation results for Scenario 2: Input + Output Noise

Model	Time (s)	RMSE value	R^2 value
LR	0.001787	2.9945	0.1686
DT	0.009995	0.8169	0.9381
RF (2)	0.020901	0.4380	0.9822
RF (3)	0.022101	0.3471	0.9888
RF (25)	0.211777	0.3690	0.9874
RF (100)	1.077512	0.3641	0.9877

Fig. 11 and Table 5 show that during stroke enter phase at t= 0.25s predicted results for all AI models shown very minimal except for LR and during stroke exist phase after t= 1.8s the RF(2,3,25) shown approximately no error however due to noise injection and overfiting nature of DT deviations can be observed. During the stroke phase LR continues to show poor results with the reference trajectory, failing to reproduce both the peak magnitude and temporal evolution of shoulder abduction. This behavior confirms that LR is fundamentally unable to model the nonlinear and phase-dependent coupling between elbow and shoulder motion, particularly under uncertainty. The DT model shows a clear reduction in accuracy compared to the noise free case during stroke phase. While the overall trajectory shape is still recognizable, localized oscillations and deviations appear near regions of rapid motion change. Fig. 12shows that DT errors have arisen because DT relies on hard threshold splits, making it sensitive

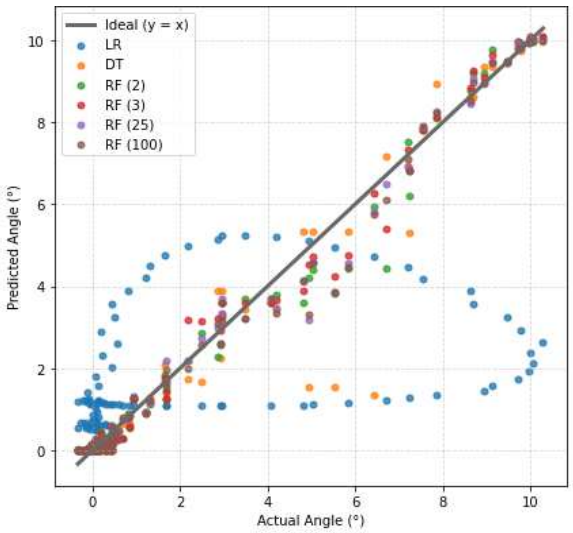


Fig. 12: Actual versus predicted angles for Scenario 2.

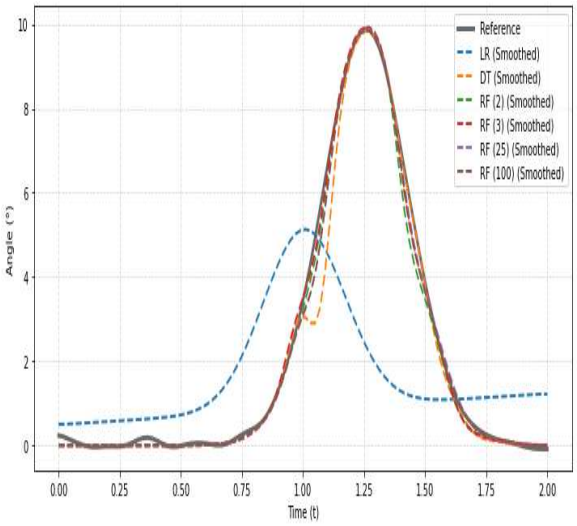


Fig. 13: Predicted shoulder abduction trajectories under Gaussian noise filtering. The reference trajectory (black) is compared with predictions obtained using Linear Regression (LR, blue), Decision Tree (DT, orange), and Random Forest (RF) models with 2 (green), 3 (red), 25 (purple), and 100 (brown) trees.

to perturbations in both input and output data. Consequently, small noise-induced variations can shift samples across decision boundaries, leading to increased prediction variance.

In contrast, RF models demonstrate strong robustness under combined noise conditions. By aggregating predictions from multiple trees trained on randomized subsets of the data, RF effectively suppresses noise induced variance and preserves the global structure of the shoulder trajectory. RF models with moderate ensemble sizes (e.g., 3 trees) achieve the best trade off between accuracy and computational efficiency with an RMSE value of 0.34 and a R^2 value of 0.988, while larger ensembles offer marginal improvements at the cost of significantly increased computation time.

3.5 Scenario 3: Gaussian Noise Filtering

Fig. 13 shows the smoothed shoulder abduction trajectories that were made by using Gaussian filtering on both the noisy reference signal and the expected outputs from Scenario 2. This phase in the procedure is conventional in biomechanics. It uses filtering to get rid of high-frequency parts that cannot be caused by human joint motion and are usually thought to be caused by sensor artifacts Sabatini (2011).

Fig. 13 and Table 6 show that during stroke enter phase predicted results for all AI models shown very minimal except for LR and during

Table 6: Evaluation results for Scenario 3: Smoothed Predictions

Model	RMSE value	R^2 value
LR	2.9042	0.1853
DT	0.4681	0.9788
RF (2)	0.2474	0.9941
RF (3)	0.1691	0.9972
RF (25)	0.2082	0.9958
RF (100)	0.2145	0.9956

stroke exist phase the RF(2,3,25) and DT shown approximately no error however due to noise filtering. During the stroke phase RF predictions match the reference trajectory almost perfectly. The error is much lower, and the predictions are more consistent over time. This finding shows that RF models can still find the underlying joint coordination structure even when they are trained under noisy conditions. It also shows that the remaining differences are mostly high-frequency artifacts instead of systematic modelling flaws. Choice After smoothing, tree forecasts get better too, although piecewise discontinuities are still there because of how tree-based models work. Linear Regression only provides a little bit of improvement because smoothing can't make up for the fact that it can't show nonlinear dynamics.

Fig. 14 shows that although gaussian noise filtering has filtered the high frequencies and made the trajectory smoother and reduced errors, as DT has a problem of overfitting, it still shows some predicting errors; however, the RF shows the best results at 3 trees due to the ensemble nature of

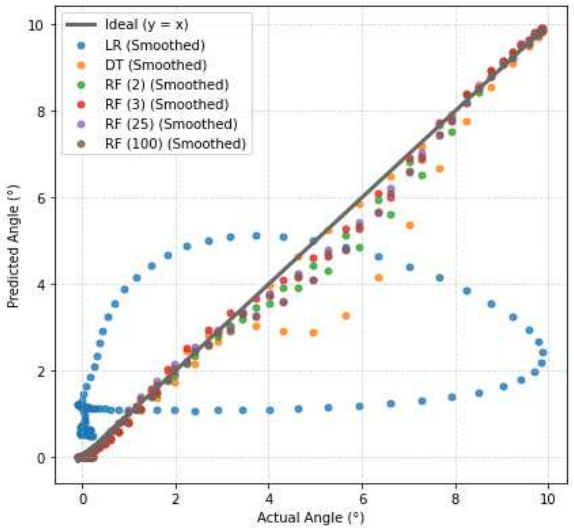


Fig. 14: Actual versus predicted angles for Scenario 3.

the algorithm, and it is more suitable for use for the controller section.

3.6 Computational Cost and Real Time Feasibility

Fig. 15 shows the summary of RMSE, R^2 values, and computational cost (sec) of all predicted results . Although the LR is not include din the figure as it has a very large value of RMSE, which retards the visibility of the chart. From Tables 4 and 5 summarize the performance of all models under both scenarios. In both cases, LR demonstrates the lowest computational time ($\sim$0.0018 s), making it highly efficient for real time implementation. However, its predictive performance is consistently poor (RMSE $\approx$ 2.97–2.99, $R^2 \approx 0.17$), confirming that it cannot capture the nonlinear

dynamics of the dataset under either noise-free or noisy conditions.

DT provides a substantial improvement in accuracy with only a minimal increase in computational cost. In Scenario 1 (noise-free), DT achieves an RMSE of 0.1627 and R^2 of 0.9975 with a computational time of 0.0091 s. In Scenario 2 (with noise), the RMSE increases to 0.8169 with R^2 of 0.9381 in 0.01 s. These results indicate that DT maintains computational efficiency while offering significantly greater robustness to noise compared to LR.

Increasing the number of trees in RF improves prediction accuracy, but at the cost of significantly longer computation times. In the noise-free scenario, for instance, RF with three trees gets an RMSE of 0.4743 in 0.029 s, while RF with 100 trees only slightly decreases to RMSE to 0.1905 but takes 0.807 s. Under noisy conditions, a similar pattern is seen, with RF (2 trees) has highest RMSE which reduces when number of trees are increased. RF (3 trees) achieving RMSE of 0.347 in 0.022 s, RF (25 trees) shown RMSE of 0.369 in 0.2s and RF (100 trees) reaching RMSE of 0.364 in 1.078 s. Based on the observed trade-off between prediction accuracy and inference latency, the three-tree Random Forest configuration was selected as the smallest ensemble achieving near-saturated prediction accuracy while maintaining prediction latency within the range required for closed-loop trajectory tracking applications.

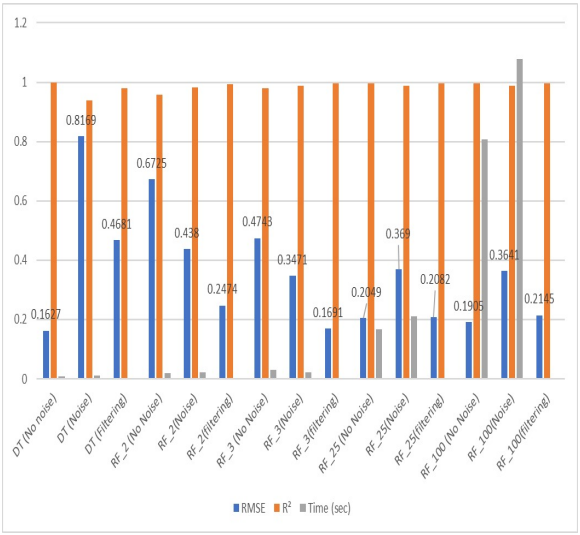


Fig. 15: Summary of RMSE value and R^2 value of all scenarios

Although the dataset represents a single front-crawl swimming motion derived from experimentally reported kinematics, model adaptability was evaluated under multiple motion-condition scenarios including noise-free, noisy, and filtered trajectory inputs. These scenarios emulate variations typically encountered in practical sensing environments and stroke execution conditions. The consistent prediction performance of small Random Forest ensembles across these scenarios indicates that the selected three-tree configuration remains stable under variations in signal quality and trajectory characteristics within the considered swimming motion framework.

4 Controller Design and Simulation

The biomechanical arm model consisting of shoulder, elbow, and wrist joints is implemented and simulated in Matlab/Simulink. To incorporate realistic biological uncertainty into the proposed control framework, biological sensory noise is added at the controller input with a magnitude consistent with reported physiological ranges. Motor noise characteristics discussed by Faisal et al. (2008). indicate noise power on the order of 1 µW, while sensory noise levels in neuromuscular systems vary with muscular strength—typically increasing for weaker muscles due to larger delays and higher variability. Reported fluctuations in sensory signal amplitude and power are approximately 1 µV and 1 µW, respectively, as noted in the Fatt and Katz (1950). Based on these established values, a 1 µW biological sensory noise component is injected into the controller input to emulate realistic neuromuscular sensing uncertainty in the model and improve physiological relevance of the control evaluation. In this study, two control strategies are employed: a Proportional–Integral–Derivative (PID) controller and a Linear Quadratic Regulator (LQR). These controllers are selected as baseline approaches due to their simplicity, well-established design frameworks, and reliable performance in practical control systems. PID provides a classical feedback control structure, whereas LQR offers an optimal control strategy based on state-space formulation. Previous studies have shown that PID and LQR controllers can effectively regulate dynamic systems with different trade-offs in response speed and robustness Saraf et al. (2020); Garziad and Saka (2019).

The controllers are evaluated for trajectory tracking of the desired shoulder joint motion. The state-space representation of the system is first verified for stability and controllability. The system poles are located in the left-half plane, indicating stability, and the controllability matrix has full rank, confirming that the system is controllable.

Proportional Integral Derivative Controller (PID)

The PID controller generates the control signal based on proportional, integral, and derivative actions applied to the tracking error. This structure allows the controller to regulate joint torques to achieve smooth tracking of the desired shoulder trajectory. The control signal $\overrightarrow{u}(t)$ is defined as Johnson and Moradi (2005):

$$\overrightarrow{u}(t) = K_p \overrightarrow{e}(t) + K_i \int_0^t e(\tau)\, d\tau + K_d \frac{de(t)}{dt} \quad (32)$$

Linear Quadratic Regulator (LQR)

The Linear Quadratic Regulator (LQR) is an optimal state-feedback control technique used

for linear time-invariant systems. It determines the optimal control input by minimizing a quadratic performance index that balances state deviations and control effort. LQR controllers have been widely applied in engineering systems such as robotics and aerospace control Fan et al. (2016); Okyere et al. (2019).

The LQR cost function is expressed as:

$$J = \int_0^\infty \left(\mathbf{x}^T\mathbf{Q}\mathbf{x} + \mathbf{u}^T\mathbf{R}\mathbf{u}\right)\, dt \tag{33}$$

where $\mathbf{x}$ is the state vector, $\mathbf{u}$ is the control input vector, $\mathbf{Q}$ is the state weighting matrix, and $\mathbf{R}$ is the control input weighting matrix.

The optimal feedback control law is given by:

$$u = -K\overrightarrow{x}(t) \tag{34}$$

To track a reference trajectory $\overrightarrow{r}(t)$, the control input becomes:

$$u = -K\overrightarrow{x}(t) + \overrightarrow{r}(t) \tag{35}$$

The optimal gain matrix is obtained by solving the continuous-time Riccati equation:

$$A^TP + PA - PBR^{-1}B^TP + Q = 0 \tag{36}$$

where A and B are the system matrices and P is the solution matrix of the Riccati equation. The feedback gain matrix K is computed as:

$$K = R^{-1}B^TP \tag{37}$$

4.1 Control implementation and Results

Figs. 16 & 17 show the simulation scheme for the state-space model of the human arm, considering the shoulder, elbow, and wrist joints, controlled with a PID controller and LQR feedback gains (K), respectively. The shoulder abduction angle in radians predicted from AI models is set as a reference input to track the shoulder angle trajectory. The controller tracks the reference value to minimize the tracking error. The results obtained from AI models are set as the reference trajectory of the shoulder joint angle for PID and LQR Controllers.

4.2 Effect of Noisy and Inaccurate AI-Based Reference Trajectories on Controller Performance

Fig. 11 shows the AI estimation of shoulder abduction angle under Gaussian noise conditions. These inputs are set as a reference trajectory to the PID and LQR controllers for LR, DT, and RF with 3 trees. RF model with three trees was selected because it provided a computationally efficient near-optimal balance between prediction accuracy and inference latency among the evaluated ensemble configurations. These trajectories are separated and converted into radians before being

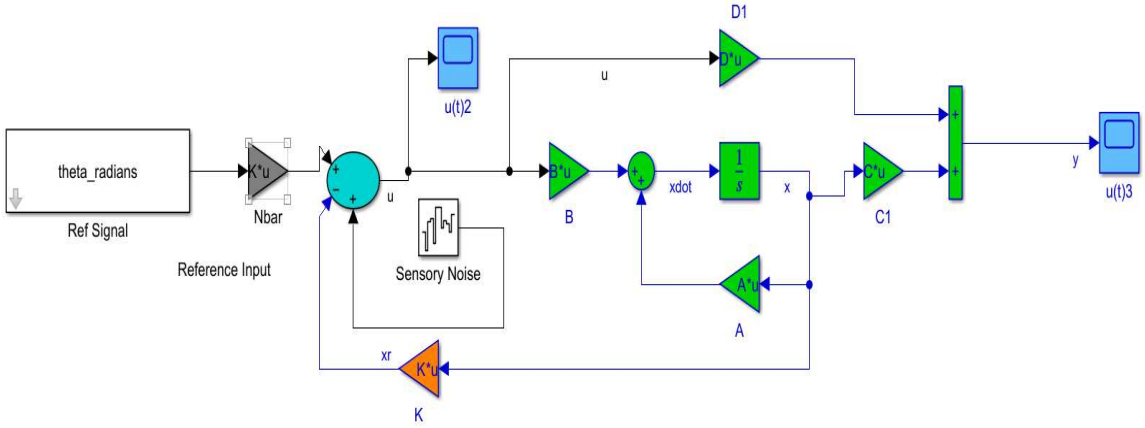


Fig. 16: Simulink Model of the biomechanical model with LQR controller with shoulder angle as reference input

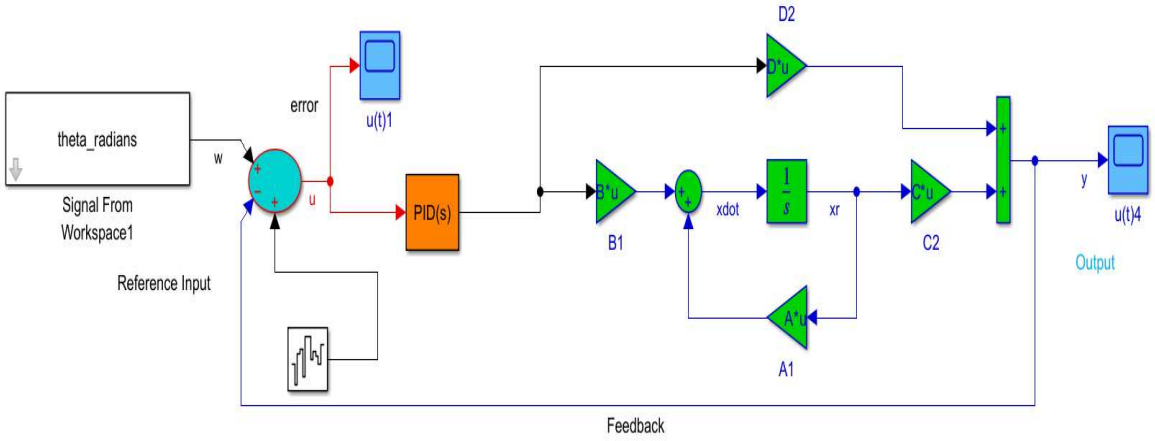


Fig. 17: Simulink Model of the biomechanical model with PID controller with shoulder angle as reference input

set as a reference signal, and after computation, they are again converted into degrees.

Fig. 18 shows the LQR tracking from the predicted results of AI models. The LQR controller experiences reduced tracking, decreased peak amplitude, and delayed reaction due to

the LR-based prediction, and due to its linear prediction nature and temporal misalignment, it underestimates the peak angle. This happens as a result of biased or noisy predictions forcing a trade-off between tracking and state regulation, which results in residual oscillations and suppressed motion. The LQR control rule minimizes a quadratic cost under the assumption of smooth and accurate references. When the DT-based prediction is employed as the reference, sharper transitions and local deviations in the anticipated trajectory propagate due to the feedback law. This results in oscillatory behavior around the motion's falling edge and overshoot close to the peak. Even moderate noise in the reference signal can impact LQR performance, as evidenced by the fact that even small prediction errors cause minor oscillations and transient deviations, even though the RF(3) based prediction offers the closest approximation to the actual shoulder trajectory in terms of amplitude and timing. To achieve optimal tracking in biomechanical applications, the LQR controller needs smooth, high-fidelity, and ideally pre-filtered prediction signals. Overall, the controller shows significant sensitivity to reference quality.

Fig. 19 shows that the AI predicted results are set as a reference to PID controllers. The PID controller is less affected by AI based references that are noisy or inaccurate, which means it is more stable when predictions are not certain.

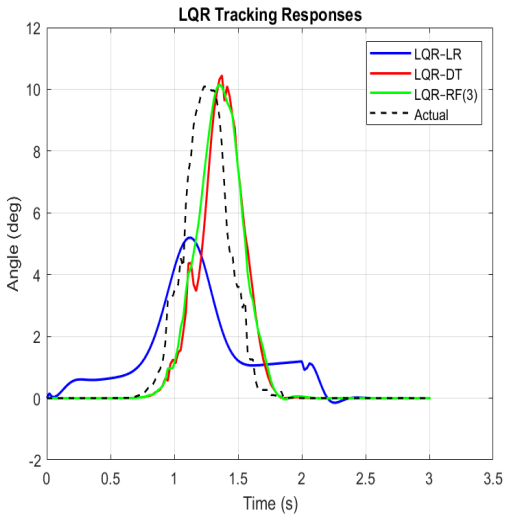


Fig. 18: PID tracking response for LR (blue), DT (red), and RF (3 trees) (green) and actual (doted)

The LR-based reference leads to less peak tracking and slower convergence. However, the integral action of the PID controller partially compensates for steady state error, which makes convergence smoother but slower than LQR. When using the DT-based prediction, sharp variations in the reference make the derivative action stronger and build up in the integral term. This causes a modest overshoot followed by an undershoot after the peak, but the overall response stays steady. When the RF(3) based prediction is used, the PID controller does a better job of tracking, with a little overshoot, a faster settling time, and a smoother convergence, even though the peak amplitude is a little lower than the actual trajectory. These observations suggest that PID control, which is based on errors rather than the best model, is

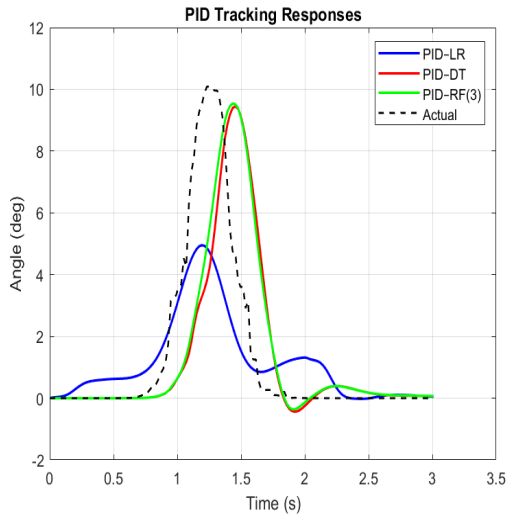


Fig. 19: PID tracking response for LR (blue), DT (red), and RF (3 trees) (green) and actual (doted)

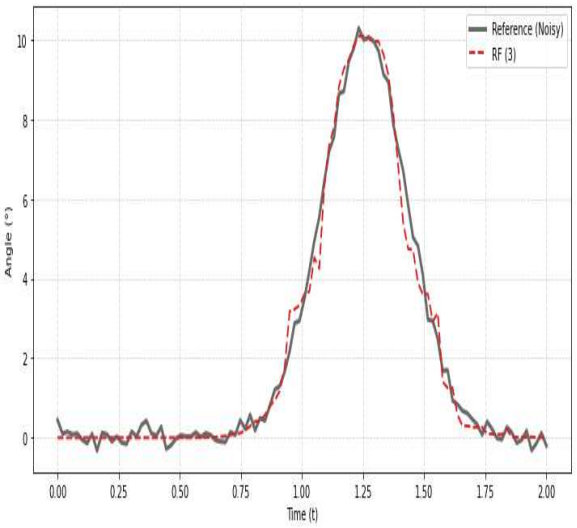


Fig. 20: RF under 3 number of trees under noisy conditions

more tolerant of noisy and defective reference signals. This means that it can still track accurately even when the forecast circumstances are bad, but it will be less accurate. The results show that bad or noisy AI predictions go straight into the control loop, which makes tracking less accurate. LQR is more sensitive to reference errors, while PID is more robust. RF(3) consistently improves the performance of both controllers by making predictions more accurate.

4.3 Shoulder Reference Trajectory Tracking using smooth noise filtered output Control

Fig. 20 shows that the best result of RF under noisy conditions resembles the reference trajectory of the shoulder joint very closely. But PID can handle noise only to some extent, and LQR performance is highly affected by reference signal noise, so a pre-filtering process is required Esmzad et al. (2025), Lahmar et al. (2025).

However, Fig. 21 shows the RF with 3 trees result after gaussian filtering done in section 3.5 which can be used as a reference trajectory for controllers for which this trajectory is converted into radians for better observation of the controller performance. The Gaussian-filtered RF(3) prediction was selected as the reference trajectory for controller validation because it achieved the lowest prediction error (RMSE $\approx$ 0.16) among the evaluated models. Since the dataset was generated from experimentally reported swimming kinematics within physiologically realistic joint ranges,

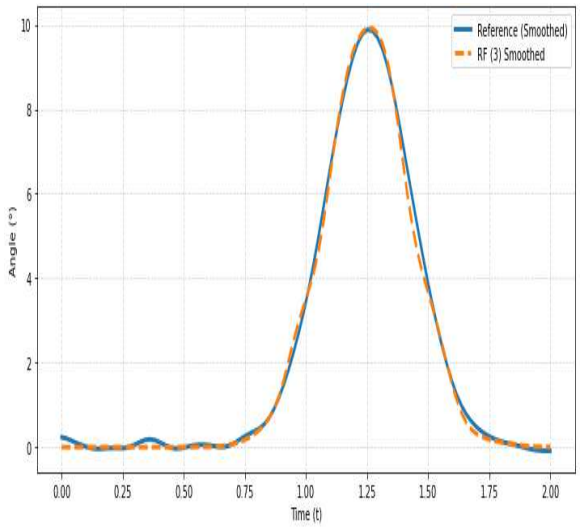


Fig. 21: Reference trajectory of shoulder angle RF under 3 trees after noise filtering

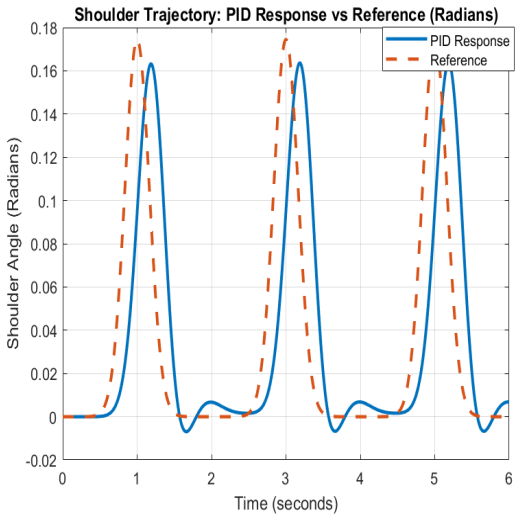


Fig. 22: Tracking of shoulder angle for a closed system with PID

this trajectory represents a biomechanically consistent approximation of realistic shoulder motion suitable for controller evaluation.

4.3.1 Results of LQR and PID Controller for smooth reference

In this section, the effectiveness of the control systems for the proposed biomechanical model is presented.

Figs. 22 & 23 show the results for the shoulder angle of the biomechanical model in front crawl swimming with LQR and PID controllers, respectively.

The PID controller exhibited a trajectory with a slightly delayed response compared to the LQR controller. This delayed response is due to the inherent nature of the PID control algorithm, which relies on feedback from the system to adjust the control input. The integral and derivative terms in the PID controller contribute to the error correction and damping, leading to a more stable

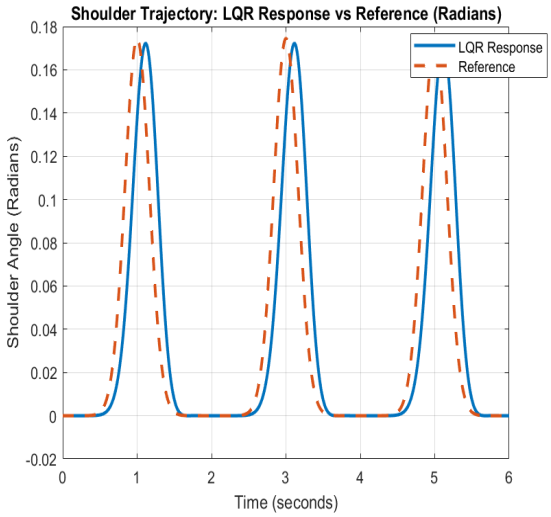


Fig. 23: Tracking of shoulder angle for the system with LQR

but slightly delayed response. The observed lower amplitude in the trajectory generated by the PID controller suggests that the controller might be overly conservative in its adjustments, resulting in a smoother but less aggressive response.

On the other hand, the LQR controller demonstrated superior performance in trajectory tracking, exhibiting a response closer to the desired trajectory with minimal delay. The LQR controller is designed to minimize a quadratic cost function, optimizing the control input over time. This optimal control strategy contributes to the more precise and timely tracking observed in the shoulder angle trajectory. The LQR controller also displayed a delayed response, but less prominent than the PID controller.

Both controllers have performed exceptionally well while catering 1 µW neuromuscular sensing uncertainty as biological sensory noise at the input side. The closed-loop controller effectively attenuates this disturbance, resulting in negligible impact on tracking performance and overall system behavior.

Fig. 24 & Fig. 25 show the error between the system response and the reference input for a system with a PID Controller and with an LQR controller (Maroon line). It can be observed that the LQR controller has a lower RMSE value than the PID controller, as shown in Table 7, indicating that LQR showed better results for the system.

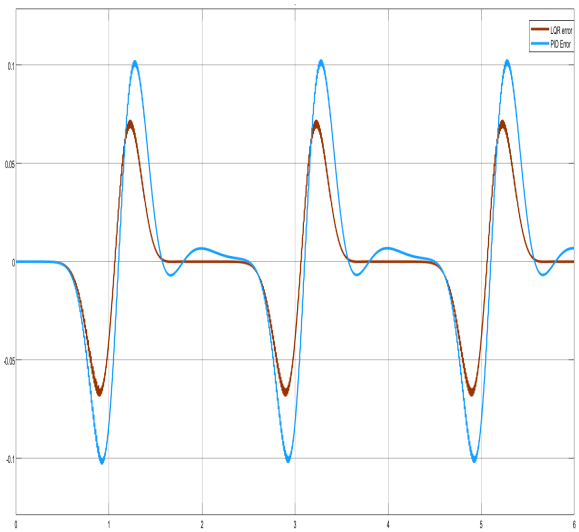


Fig. 24: Error plot for LQR and PID response for the system

Furthermore, ripples in the trajectory generated by the PID controller may be attributed to the oscillatory nature of the proportional and derivative terms. The PID controller's attempt to

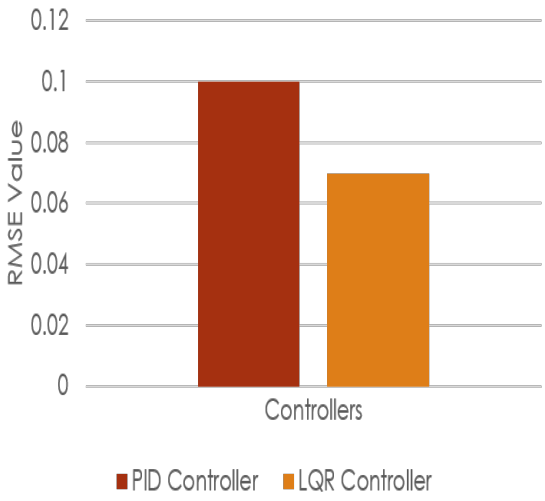


Fig. 25: Error graph for LQR and PID response for the system

Table 7: Properties of system with LQR and PID Controller

Comparison Parameter	PID	LQR
Maximum θ_1 (rad)	0.162	0.172
Minimum θ_1 (rad)	-0.006	0
Maximum Error (rad)	0.00175	0.00125
Minimum Error (rad)	-0.00175	-0.00125
RMSE value	0.1	0.07

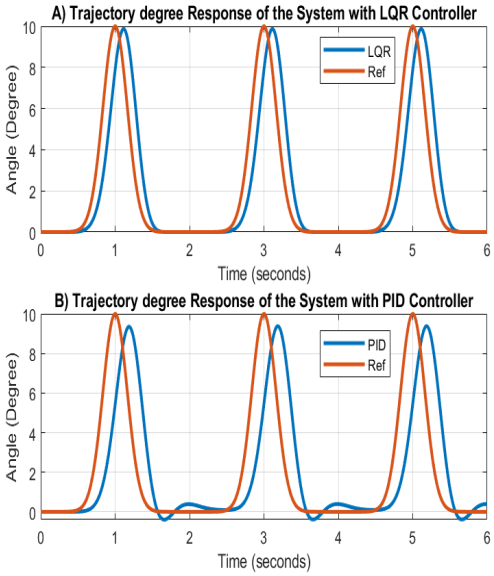


Fig. 26: Output Response of the system in degrees

rapidly correct errors could result in overshooting and oscillations, contributing to the observed ripples in the trajectory. In contrast, the LQR controller's optimization approach may have mitigated such oscillations, resulting in a smoother trajectory.

In Fig. 26, the output shoulder angles are converted back into degrees and show the results in degrees, as the dataset generated has angles

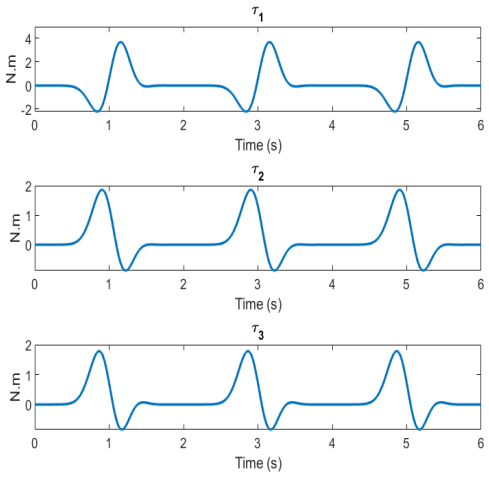


Fig. 27: Joint Torques for Shoulder (τ_1), Elbow (τ_2) and Wrist Joint (τ_3) of the proposed model with LQR controller

in degrees. The results for both LQR and PID controllers used in biomechanical systems showed acceptable results; however, the LQR controller showed better results than the PID controller in the system.

Table 8: Joint Torques of the system with LQR controller

Joints	Max τ (N-m)	Min τ (N-m)
Shoulder Joint	4	-2
Elbow Joint	2	-1
Wrist Joint	2	-1

As the LQR controller displayed better performance than the PID controller in this biomechanical model, a system with LQR is used to study the effect of joint torques on arm movement in swimming. Fig. 27 and Table 8 show the arm joint

torque for each joint, i.e., Shoulder (τ_1), Elbow (τ_2), and Wrist Joint (τ_3). The study conducted by (O'sullivan et al. 2022) estimated the mean torque that can be exerted by the shoulder and elbow, i.e., 47.69 N·m and 44.18 Nm. In our model, as we are using limited flexion motion of 10°, it therefore exerts a maximum torque of 4 N·m and 2 N·m for the elbow and wrist joint, which are under the torque limit of the shoulder. The magnitude of force or torque exerted by the shoulder joint is higher than that on the elbow and wrist joints throughout various phases of swimming. Consequently, the dynamic and intricate movements of the arms during swimming place a comparatively higher stress level on the shoulder joint, as high propulsive forces are produced when the shoulder joint is in motion. This leads to the inference that the shoulder joint is inherently more vulnerable within the framework of arm movements during swimming. Therefore, the shoulder joint is most exposed and can lead to injury.

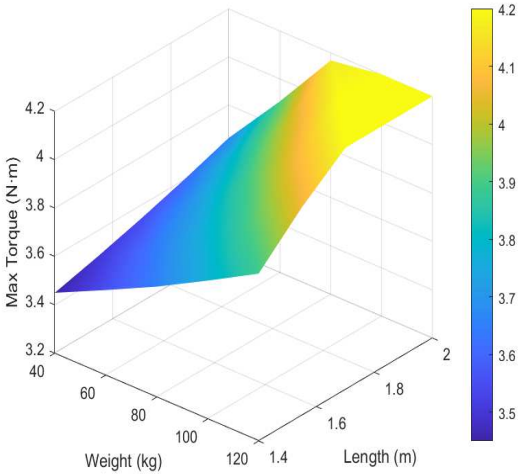


Fig. 28: Effect of variation in body weight and length in shoulder torque (τ_1)

4.4 Effect of Anthropometric Variations on Joint Dynamics and Torque Requirements

To evaluate the influence of inter-individual anthropometric variability on joint dynamics, body weight (W) and body length (L) were varied within physiologically realistic ranges. These global anthropometric parameters directly affect the mass and length of individual limb segments through the scaling relationships defined in equation (10 to 15). As a result, variations in W and L propagate into the segmental moments of inertia and inertial coupling terms of the biomechanical model.

Fig. 28 illustrates the resulting variation in maximum required shoulder joint torque as a function of body weight and body length. Across the investigated range, the maximum torque increases from approximately 3.4 N·m for lighter and shorter individuals to approximately 4.2 N·m for heavier and taller individuals. This demonstrates that anthropometric variability induces non-negligible changes in joint dynamics and torque demand, even when identical reference trajectories are used.

It is essential to remember that while the PID and LQR controllers used in this study are fixed-gain controllers, they do not specifically account for modelling uncertainty brought on by inter-individual variability. The resulting torque demands for repetitive swimming motions are nevertheless well under the physiological shoulder torque limitations observed in experiments, despite this constraint. This shows that even without adaptive gain tuning, the suggested control system maintains joint safety and practicality under a variety of anthropometric situations.

5 Performance Comparison

5.1 Model Comparison with Previous Studies

The estimated results by RF and DT, as shown in Figure 11 and Figure 13, are close to the estimated value as given in the experimental work performed by Ichikawa et al. (2003). The evaluation parameters listed in Table 9 are presented for input & output noise conditions to replicate a real-world scenario in which different noise is added.

A side-by-side summary of the suggested framework and earlier research is presented in Table 9. This comparison aims to contextualize the performance of the proposed AI-based inference and control framework, not to claim superiority over fully experimental measurement methods. Unlike previous studies that use wearable inertial sensors or videography, the present study uses a simulation-based dataset generation method based on empirically determined joint kinematics, which allows for a controlled analysis of noise sensitivity and learning behavior.

Table 9: Comparison of current study results with literature

Literature	**Methodology**	**RMSE**	R^2
Current Study	LR	2.99	0.16
	DT	0.81	0.93
	RF (3)	0.34	0.98
	LQR	4 (0.07 rad)	-
	PID	5 (0.1 rad)	-
(Fantozzi et al. 2016)	IMMUs	6 to 10	0.95
(Guignard et al. 2021)	IMMUs	-	-
(Boyer et al. 2020)	Data fusion	1.6 to 11.24	0.90
(Macaro et al. 2018)	ANN	7.75	-
(Yanai et al. 2000)	Videography	13%	-

The current study confirms that linear models are inadequate for explaining the nonlinear interaction between elbow motion and shoulder abduction during front crawl swimming since Linear Regression (LR) exhibits unsatisfactory prediction performance (RMSE = 2.99°, $R^2 \approx 0.16$.). Errors are significantly lower in the Random Forest (RF) and Decision Tree (DT) models. In noisy environments, the RF model with three trees offers the optimum balance between robustness and accuracy RMSE = 0.34°, $R^2 \approx 0.98$. These results imply that in the presence of measurement uncertainty, ensemble based nonlinear models are better at explaining interjoint interactions.

Compared to IMU based experimental studies, the RMSE values reported in the literature are much higher. (Fantozzi et al. 2016) showed that the correlation values were around 0.95 and the RMSE values ranged from 6° to 10° when upper limb joint angles were estimated using inertial measurement units. Significant variability and uncertainty in IMU based shoulder angle estimation while swimming were emphasized by (Guignard et al. 2021), demonstrating the challenges associated with sensor positioning, soft tissue artifacts, and the shoulder joint's multi-degree of freedom features. These discrepancies demonstrate how challenging it is to ascertain shoulder kinematics in actual aquatic conditions, not that the proposed framework is superior to experimental sensing technologies.

With RMSE values ranging from 1.6° to 11.24° and R^2 values ranging from 0.9 to 0.99, depending on the sensor configuration and task difficulty, data fusion approaches released by (Boyer et al. 2020) demonstrate a wide range of performance. Similarly, using artificial neural networks, (Maccaro et al. 2018) discovered an RMSE of about 7.75°. This demonstrates that the primary sources of inaccuracy in data-driven biomechanical models continue to be experimental noise and subject variation.

Despite providing important biomechanical insights, videography based methods, as demonstrated by (Yanai et al. 2000), yield errors of about 13% and require specialized equipment, controlled experimental settings, and extensive post processing. Instead of trying to reproduce the whole complexity of real data collection, the current study focuses on a controlled synthetic dataset to methodically evaluate the learning behavior of AI models under certain noise settings.

The combination of AI-based prediction and control-focused assessment is a distinctive characteristic of the proposed system. The majority of earlier studies have concentrated on measuring accuracy. The effectiveness of expected trajectories as reference inputs for control is examined in this work. Even trajectories that are estimated from noisy data can be effectively managed, as demonstrated by the tracking errors of roughly 0.07 rad for the LQR controller and 0.1 rad for the PID controller. This emphasizes how important the suggested dataset is as a testing ground for swimming biomechanics controller design and validation.

The results in Haghpanah et al. (2023), which found that the shoulder joint is more vulnerable to high torque during swimming, are consistent with the demonstrated accuracy of AI models in this study. The development of real time feedback systems that can alert swimmers when their

joints are at the incorrect angle or under excessive stress, thereby increasing their risk of injury, is encouraged by the study's exceptional accuracy in predicting shoulder movements. By focusing on metrics like RMSE and R^2, this work also demonstrates the utility of this technique. These steps ensure that the models are both theoretically valid and applicable to real-world swimming scenarios, which are constantly changing.

Overall, the comparison in Table 9 indicates that this study's primary contribution is to provide a repeatable, noise-aware framework for testing AI-based interjoint inference and control algorithms, rather than to replace experimental measurement systems. By generating synthetic data based on experimentally reported kinematic ranges and systematically adding noise, the proposed method links analytical modelling with future experimental applications of wearable sensor technology.

5.2 Validation of torque profile achieved

Table 10 presents a comparison of the estimated joint torque magnitudes against data from previous experiments and estimations. The current model generates peak torques of around 4 N·m the shoulder, 2 N·m the elbow, and 2 N·m the wrist while performing front crawl swimming as shown in Fig. 27. These values are compared with literature studies that obtained joint torques through fundamentally different methodologies. Specifically, (Riani et al. 2018) found that the torques at the shoulder, elbow and wrist joints were approximately 22 N·m, 7 N·m and 1 N·m respectively, in an exoskeleton designed for rehabilitation. In a comparable study, (Batalha et al. 2012) employed a Biodex isokinetic dynamometer to assess peak torques of the shoulder rotators ranging from 21 to 37 Nm. Participants performed maximal voluntary internal and external rotations while seated, demonstrating their near maximal muscular capacity rather than task specific swimming loads. Conversely, (O'sullivan et al. 2022) determined the maximum torques for the shoulder and elbow (47.69 N·m and 44.18 N·m, respectively) by regression models utilizing dynamometer-measured data and anthropometric characteristics, therefore establishing population-level upper limits for joint torque generation.

Table 10: Validation of joints torque

Source / Joints	τ_1 **(Nm)**	τ_2 **(Nm)**	τ_3 **(Nm)**
Current Study	4	2	2
(Riani et al. 2018)	22	7	1
(Batalha et al. 2012)	21–37	–	–
(O'sullivan et al. 2022)	47.69	44.18	–

The calculated peak joint torques in this study—4 N·m for the shoulder and 2 N·m for the elbow—are lower than the values reported in prior studies in Table 10 , which measured torques under different tasks such as rehabilitation exoskeleton use Riani et al. (2018), maximal voluntary rotations Batalha et al. (2012), and population-level dynamometer assessments O'sullivan et al. (2022) with high range of motion (RoM) out model has limited RoM i.e. shoulder between 0° to 10°. and elbow 0° to 80° which impact the perf. While hydrodynamic forces and detailed muscle-tendon dynamics are outside the scope of the present work, their exclusion reduces torque estimates. Combined with the planar 3-DOF representation limiting out-of-plane contributions, the predicted torques correspond to approximately 8% to 29% of the values reported in these studies. This demonstrates that the lower torques are a direct and expected consequence of the modelling simplifications rather than a lack of physiological validity.

Compared to these maximal or near-maximal reference values, the torques predicted by the present swimming model remain substantially lower, which is expected given the sub-maximal, repetitive nature of swimming. The model preserves the experimentally confirmed hierarchy of joint loading, with the shoulder exhibiting the highest torque requirement, followed by the elbow and wrist. This comparison indicates that the anticipated torque profiles remain within the physiological constraints established by experimental findings. This corroborates the notion that the suggested model is applicable for biomechanical analysis of swimming.

5.3 Experimental Validation of Dataset

Although no new experimental measurements were conducted in the present study, the generated shoulder and elbow joint angle dataset is strongly grounded in and validated against experimentally established biomechanical evidence reported in the swimming kinematics literature. The analytical joint trajectories adopted in this work originate from the formulation proposed by (Ichikawa et al. 2003), in which joint angle time histories were derived directly from experimentally measured upper limb kinematics obtained using synchronized underwater and above water video motion analysis. In this study 2 segments of the upper body upper arm and the forearm is used for the estimation of angle profiles of upper arm During which 4 well trained subjects was used to perform front crawl swimming stroke in swimming pool of 50 m for 3 times at different stroke speed of low, medium and fast, there movement was recorded by accelerometer and through video camera. The study focused on the movement profile of left-hand shoulder abduction, shoulder extension, and elbow

flexion angle. The dataset acquire in the current study shows Gaussian-shaped joint profiles which strongly mimic these experimental results of the experiment.

The experimental validity of the present data set is further supported by a comparison with the upper limb kinematic assessment framework based on IMUs proposed by Fantozzi et al. (2016), which represents one of the most comprehensive experimental validations of joint kinematics related to swimming using wearable sensors. In this experiment, eight subjects of age 25 ± 3.4 years are used, of height of 182±8 cm and a mass of 77±10 Kg, to perform twenty strokes of front crawl and breast stroke swimming in a controlled laboratory environment. This study modelled the upper limb as an open kinematic chain consisting of the thorax, upper arm, forearm, and hand, along with 7 degrees of freedom in interjoint coordination patterns. The equipment used in this experiment was a wearable inertial magnetic measurement unit (IMMU) system (APDM Opal) consisting of seven sensor units, sampled at 128 Hz to obtain the movement profiles of joints. the IMMU based framework inherently contains experimental noise, arising from sensor drift and bias, magnetic disturbances, Soft tissue artifacts, and misalignment between anatomical and sensor frames. A Kalman-based sensor fusion algorithm was used to minimize RMSE with respect to optical motion capture. In present study we use this approach to model gaussian noise of 10% to mimic the real word sensor noise and the use gaussian kernel filtering to tackle this noise estimated this encourage from study conducted by (Jeon and Lee 2024) on IMU based gait and kinematic data augmentation injected Gaussian noise at approximately 10% of the feature range or standard deviation, effectively simulating realistic sensor fluctuations and enhancing model robustness to real world disturbances.

Table 11 shows the Range of Motion (ROM) of joints in the current study, along with validation through experimental literature. It can we well observed that the ROM of the shoulder and elbow joint falls within the experimental ROM conducted in these two studies. It can be defined that the age limit of our more and these experimental more are approximately validated.

Table 11: Range of Motion of Upper-Limb Joints Reported in Literature

Study/ROM(°)	**Age**	**Shoulder**	**Elbow**
Current Study	25 - 43	0 -1 0	0-80
(Ichikawa et al. 2003)	–	−3 - 10	12 - 80
(Fantozzi et al. 2016)	25 ± 3.4	−20 - 18	5 - 82

To account for inter-individual variability and age-related changes in neuromuscular performance, the dataset incorporates a gradual reduction in joint excursion, temporal characteristics, and curvature parameters based on an established

annual performance decline rate reported in longitudinal swimming studies. This age-dependent scaling is consistent with experimentally observed reductions in joint mobility, force generation capacity, and movement speed in adult swimmers, further reinforcing the physiological realism of the generated data across the considered age range (25–43 years). The dataset captures the dominant stroke relative joint behavior during propulsion by taking the age factor and noise estimation so it is therefore suitable for methodological feasibility analysis. The resulting synthetic dataset is considered experimentally consistent at the trend and range levels, providing a reliable basis for evaluating AI-based joint angle prediction and control strategies under simplified but experimentally grounded conditions.

6 Discussion and Implications

present study provides a mechanistic evaluation of upper limb biomechanics in front crawl swimming by integrating biomechanical modelling, AI-based kinematic inference, and control-based trajectory tracking. Rather than only reporting performance outcomes, the analysis focuses on understanding how interjoint dynamics, prediction uncertainty, and control strategies interact to influence joint torque generation and motion tracking behavior.

6.1 Study Contribution and Methodological Insights

This study investigates upper limb biomechanics in front crawl swimming through an integrated framework combining biomechanical modelling, machine learning–based joint estimation, and control-based trajectory tracking. The primary contribution lies in analysing how biomechanically grounded motion generation, AI-based interjoint prediction, and trajectory tracking interact within a unified framework under sensing uncertainty, with particular emphasis on how prediction uncertainty propagates into control performance.

The dataset used in this study was synthetically generated based on experimentally reported swimming kinematics while respecting physiologically reported ranges of motion and joint torques (Subsection 5.3). To emulate realistic sensing conditions, Gaussian noise (10%) was introduced into the data, and the AI models were evaluated under noise-free, noisy, and noise-filtered scenarios (Subsection 3.3 to 3.5). The resulting performance variations demonstrate that the models respond to measurement uncertainty rather than simply reproducing predefined trajectories. Three machine learning models, LR, DT, and RF, were evaluated to analyze their ability to capture interjoint kinematic relationships. The inferior performance of LR highlights the fundamentally nonlinear coupling between elbow and

shoulder motion, which cannot be represented through linear mappings. DT models achieve high accuracy in noise-free conditions due to their ability to learn precise threshold-based relationships; however, their reliance on hard splits makes them highly sensitive to small perturbations in input data. In contrast, RF models demonstrate improved robustness under noisy conditions due to their ensemble structure, where multiple decorrelated trees reduce variance through averaging. This behavior is particularly relevant in biomechanics, where measurement uncertainty arising from soft tissue artifacts and sensor noise is unavoidable. The diminishing performance gains observed with increasing tree numbers further indicate that moderate ensemble sizes are sufficient to capture the dominant interjoint dynamics without incurring unnecessary computational cost.

The predicted shoulder angles were subsequently used as reference inputs for PID and LQR controllers within the biomechanical arm model. The results demonstrate that controller performance is strongly influenced by the quality of AI-generated reference trajectories, highlighting a direct coupling between prediction uncertainty and control behavior. From a control theoretic perspective, the LQR controller achieves smoother and more precise tracking because it minimizes a quadratic cost function that balances state deviation and control effort, resulting in optimized torque profiles. However, this optimal formulation also makes LQR more sensitive to AI-predicted uncertainties in the reference signal, as deviations propagate through the state-feedback structure. In contrast, the PID controller, which relies on error-driven feedback, exhibits greater tolerance to AI predicted uncertainties inputs but produces slower and less precise tracking due to its reactive nature.

From a biomechanical standpoint, this sensitivity has important implications. Noisy or inaccurate shoulder trajectory predictions can lead to improper torque generation, potentially increasing mechanical loading on the joint and contributing to fatigue or injury risk during repetitive swimming motion. The application of Gaussian filtering improves trajectory smoothness by removing high-frequency components that are not physiologically realistic, thereby enhancing both control stability and biomechanical plausibility of the motion. Both controllers exhibit strong input neuromuscular sensory noise rejection, ensuring stable system performance despite measurement fluctuations of 1 micro Watt.

The analysis of joint torque distribution further reveals that the shoulder joint consistently experiences higher torque compared to the elbow and wrist joints. This can be explained biomechanically by the shoulder's role as the primary driver of upper limb propulsion in swimming. The shoulder joint has a larger effective moment arm

and must accelerate the mass of the entire distal limb segments, resulting in higher torque demand. Additionally, its greater moment of inertia amplifies the required control effort during dynamic motion. This observation is consistent with established findings in swimming biomechanics, where the shoulder contributes the majority of propulsive force and is therefore more susceptible to mechanical loading and overuse injuries.

6.2 Comparison with Existing IMU and Video-Based Motion Analysis Methods

Motion analysis in swimming commonly relies on wearable inertial measurement units (IMUs) or video-based motion capture systems. IMU-based sensing enables real-time monitoring of joint kinematics and stroke parameters, but accurate estimation of shoulder motion requires precise sensor placement, calibration, and drift compensation. In aquatic environments, waterproofing requirements and soft-tissue motion can further affect measurement accuracy Morais et al. (2022); Vieira et al. (2024).

Video-based and vision-based approaches can provide detailed spatial information of upper limb motion without requiring body-mounted sensors. However, underwater camera systems are typically expensive, require controlled lighting and camera placement, and often involve extensive post-processing. Their reliability may also be affected by occlusion, refraction, and limited camera coverage Van Crombrugge et al. (2022).

The framework proposed in this study aims to complement these approaches by exploring a data-driven method for estimating shoulder kinematics from elbow motion. By learning the inter-joint coupling between elbow and shoulder movements, the approach reduces reliance on extensive sensing infrastructure while maintaining competitive predictive accuracy. Such model-based and learning-based strategies are increasingly investigated to support scalable motion analysis in sports environments where cost, deployability, and robustness are important considerations.

The present findings can be compared with the work of Haghpanah et al. (2023), where a nonlinear upper limb model with adaptive sliding mode control was employed. Their approach demonstrated strong robustness to model uncertainties due to the inherent switching nature of sliding mode control. In contrast, the linear controllers used in this study (PID and LQR) exhibit sensitivity to reference inaccuracies and modelling assumptions. However, the current work introduces an additional dimension by explicitly integrating AI-based trajectory prediction into the control loop, thereby revealing how prediction uncertainty influences control performance,

an aspect not addressed in prior studies. This comparison highlights a trade off between robustness offered by nonlinear control methods and the interpretability and simplicity of linear control frameworks combined with data-driven estimation.

6.3 Practical Implications and Future Applications

Although the present study is conducted in a simulation environment, the results provide useful insights into the relationship between joint kinematics, torque requirements, and controller performance during swimming motion.

Analysis of joint angle trajectories in conjunction with torque profiles provides insight into the trade-off between movement accuracy and mechanical loading. From a biomechanical perspective, achieving precise trajectory tracking at the cost of excessive torque may increase joint stress and fatigue, whereas overly conservative control may reduce propulsion efficiency. Therefore, the observed balance between smooth tracking (LQR) and robustness (PID) reflects a fundamental trade-off between control optimality and physiological safety, which is critical in repetitive athletic motions such as swimming.

Computational cost analysis indicates that lightweight models such as Decision Trees and small Random Forest ensembles exhibit low prediction latency. This suggests that the proposed framework could potentially be integrated with wearable sensing technologies in future experimental studies to estimate shoulder kinematics and joint loading during swimming practice.

It is important to emphasize that the present work does not claim direct improvements in swimmer performance or injury prevention. Instead, it establishes a structured framework for analysing upper limb biomechanics and control behaviour under sensing uncertainty. Future experimental validation and integration with real sensing systems may enable practical applications in technique monitoring, performance analysis, and rehabilitation-oriented swimming research.

7 Limitations

Despite the insights provided by the proposed framework, several limitations must be acknowledged. The most significant limitation is the absence of validation using real experimental swimming data. The dataset used in this study is synthetically generated based on experimentally reported kinematic patterns and physiological constraints, but it does not include motion capture or in-water measurements obtained from human participants. The noise model used in this study is limited to Gaussian perturbations and

does not reflect complex real-world sensing conditions such as sensor drift, magnetic interference, and soft tissue artifacts. Consequently, although the simulation results demonstrate the feasibility of the proposed AI–control framework, the findings cannot yet be considered experimentally validated. Furthermore, the evaluation of AI models and controllers was conducted in an offline simulation environment. Real-time implementation challenges, including communication delays and wearable device constraints, were not investigated in this work.

8 Future Work

Future research will focus on validating the proposed framework using experimentally acquired swimming data. Integration with wearable IMU sensors or underwater motion capture systems will enable evaluation of AI-based shoulder estimation and control strategies under real aquatic conditions. Future work will extend the proposed framework to multiple swimming styles and subject-specific motion datasets to further evaluate the generalization capability of the learning-based joint prediction model across broader biomechanical motion conditions. Additionally, the biomechanical model does not account for complex physiological factors such as muscle activation dynamics, soft tissue effects, and hydrodynamic interactions, which may be incorporated in the future.

Another important direction is the incorporation of subject-specific biomechanical parameters and model musculoskeletal dynamics to better capture physiological variations among swimmers. Adaptive or robust control strategies may also be explored to improve trajectory tracking performance under parameter uncertainty and measurement disturbances.

Finally, the proposed framework may be extended toward practical training and rehabilitation applications by integrating real-time feedback mechanisms capable of monitoring shoulder kinematics and joint loading during swimming practice.

9 Conclusion

This study presented a biomechanically grounded and noise-aware simulation framework that integrates reduced-order upper limb modelling, AI-based interjoint inference, and classical control strategies to investigate shoulder trajectory estimation and tracking in front crawl swimming. Synthetic joint trajectories and torque profiles were generated within physiologically reported ranges derived from validated video- and IMU-based studies, enabling controlled evaluation of learning and control performance under sensing uncertainty.

The results demonstrate that interpretable AI models, particularly small Random Forest ensembles, can effectively capture the nonlinear coupling between elbow and shoulder motion and provide feasible reference trajectories for control systems. Controller performance was strongly influenced by the quality of these AI-generated references. Noisy or inaccurate predictions reduced tracking performance, highlighting the importance of reliable prediction and signal conditioning.

Between the evaluated controllers, the LQR controller achieved smoother and more precise trajectory tracking, while the PID controller exhibited comparatively higher oscillatory behavior. However, both controllers show limited capability in handling model uncertainties, suggesting that adaptive or robust control strategies may provide further improvements in future studies. Overall, the proposed framework provides a structured simulation platform for analysing AI–control interaction, robustness to sensing noise, and joint loading behavior in swimming biomechanics. By linking joint trajectory estimation with torque-based control analysis, the study establishes a methodological foundation for the development of data-driven approaches to technique monitoring and biomechanical analysis in aquatic sports.

However, due to the reliance on synthetic data, simplified biomechanical modelling, and the absence of experimental validation, the present findings should be interpreted as preliminary. The applicability of the proposed framework to real-world swimming conditions may be limited by unmodelled factors such as complex hydrodynamic interactions, subject-specific variability, and real sensor noise characteristics. Experimental validation using in-water measurements will be necessary to confirm the practical utility of the proposed approach.

Declarations

- Funding: The authors have not received any funding.
- Conflict of interest/Competing interests: The authors declare that there is no competing financial interest or personal relationship that could have appeared to influence the work reported in this paper.
- Ethics approval and consent to participate: Not applicable
- Consent for publication: Taken from all authors
- Data availability: Yes, dataset is available as supplementary material.
- Materials availability: Not applicable
- Code availability: Will be provided on request
- Author contribution:

  Z.S.: Conceptualization, Writing original manuscript, Methodology, Investigation, Software, Data Curation.

M.I.: Conceptualization, Writing original manuscript, Supervision, Formal analysis, Validation, Resources.

J.I.: Conceptualization, Reviewing original manuscript, Supervision, Formal analysis, Validation, Resources.

References

Ardister J, Geddes J, Feeny BF, et al (2025) Modeling and computational fluid dynamics validation of a nonholonomically constrained two-rigid-body swimming system. arXiv preprint arXiv:250904670

Astawa NNAMP, Darmawijaya IP, Vitalistyawati LPA (2023) The relationship of shoulder flexibility to swimming speed in teenage beginner swimmers. JOURNAL RESPECS (Research Physical Education and Sports) 5(1):10–14

Batalha NMP, Raimundo AMdM, Tomas-Carus P, et al (2012) Shoulder rotator isokinetic strength profile in young swimmers. Revista Brasileira de Cineantropometria & Desempenho Humano 14:545–553

Bedi A, Rodeo SA (2009) Os acromiale as a cause for shoulder pain in a competitive swimmer: a case report. Sports Health 1(2):121–124

Behjati Ashtiani M, Freidouny M, Ojelade A, et al (2024) Predicting external hand forces during overhead work: An approach using emg and random forest regression. In: Proceedings of the Human Factors and Ergonomics Society Annual Meeting, SAGE Publications Sage CA: Los Angeles, CA, p 10711813241264257

Bishop CM, Nasrabadi NM (2006) Pattern recognition and machine learning, vol 4. Springer

Borlaug ILG, Gravdahl JT, Sverdrup-Thygeson J, et al (2019) Trajectory tracking for underwater swimming manipulators using a super twisting algorithm. Asian Journal of Control 21(1):208–223

Bouvet A, Pla R, Delhaye E, et al (2024) Profiling biomechanical abilities during sprint front-crawl swimming using imu and functional clustering of variabilities. Sports Biomechanics pp 1–21

Boyer M, Frasie A, Bouyer L, et al (2020) Development and validation of a data fusion algorithm with low-cost inertial measurement units to analyze shoulder movements in manual workers. arXiv preprint arXiv:201007450

Breiman L (2001) Random forests. Machine learning 45:5–32

Cain SM, Morrow MM (2025) Quantifying shoulder motion in the free-living environment using wearable inertial measurement units: Challenges and recommendations. Journal of Biomechanics p 112589

Carnevale A, Longo UG, Schena E, et al (2019) Wearable systems for shoulder kinematics assessment: A systematic review. BMC musculoskeletal disorders 20(1):546

Chainok P, de Jesus K, Coelho L, et al (2023) Modeling and predicting the backstroke to breaststroke turns performance in age-group swimmers. Sports Biomechanics 22(12):1700–1721

Chhabra A, Venepally JR, Kim D (2021) Measurement noise covariance-adapting kalman filters for varying sensor noise situations. Sensors 21(24):8304

Clément J, Charbonneau M, Thompson M (2021) Instantaneous velocity estimation for the four swimming strokes using a 3-axis accelerometer: Validation on paralympic athletes. Journal of Biomechanics 117:110261

Cop CP, Cavallo G, van't Veld RC, et al (2021) Unifying system identification and biomechanical formulations for the estimation of muscle, tendon and joint stiffness during human movement. Progress in Biomedical Engineering 3(3):033002

Costa M, Barbosa TM (2018) A comparison of the evidence produced in sport science and swimming between 2013 and 2017. In: XIIIth International Symposium on Biomechanics and Medicine in Swimming: Book of Abstracts, BMS, pp 95–96

Deschodt V, Arsac L, Rouard A (1999) Relative contribution of arms and legs in humans to propulsion in 25-m sprint front-crawl swimming. European journal of applied physiology and occupational physiology 80:192–199

Dos Santos YS, Rossato M, Carneiro NB, et al (2024) Magnitude and direction of shoulder torque asymmetries between different angular velocities in competitive swimmers. Sports Biomechanics pp 1–15

El-Gohary M, McNames J (2012) Shoulder and elbow joint angle tracking with inertial sensors. IEEE Transactions on Biomedical Engineering 59(9):2635–2641

Elliott B (1999) Biomechanics: an integral part of sport science and sport medicine. Journal of Science and Medicine in Sport 2(4):299–310

Esmzad R, Sankar GS, Han T, et al (2025) Direct data driven control using noisy measurements. arXiv preprint arXiv:250506407

ExRx.net (2019) Mean segment weights. Online, URL https://exrx.net/Kinesiology/Segments, accessed: 2019-04-04

Faisal AA, Selen LP, Wolpert DM (2008) Noise in the nervous system. Nature reviews neuroscience 9(4):292–303

Fan B, Sun J, Yu Y (2016) A lqr controller for a quadrotor: Design and experiment. In: 2016 31st Youth Academic Annual Conference of Chinese Association of Automation (YAC), IEEE, pp 81–86

Fantozzi S, Giovanardi A, Magalhães FA, et al (2016) Assessment of three-dimensional joint kinematics of the upper limb during simulated swimming using wearable inertial-magnetic measurement units. Journal of Sports Sciences 34(11):1073–1080

Fatt P, Katz B (1950) Some observations on biological noise. Nature 166(4223):597–598

Fonseca JC, da Costa Souza H, da Costa Silva A, et al (2025) The use of opensim software for biomechanical modeling of the shoulder joint: a scoping review. Computers in Biology and Medicine 196:110742

Formica D, Charles SK, Zollo L, et al (2012) The passive stiffness of the wrist and forearm. Journal of neurophysiology 108(4):1158–1166

Funk L (2023) Biomechanics of the shoulder. In: Shoulder Arthroscopy: Principles and Practice. Springer, p 17–32

Gabela J, Kealy A, Li S, et al (2019) The effect of linear approximation and gaussian noise assumption in multi-sensor positioning through experimental evaluation. IEEE Sensors Journal 19(22):10719–10727

Garziad M, Saka A (2019) A comparative assessment between lqr and pid strategies in control of two wheeled vehicle. International Journal of Engineering Research in Africa 43:59–70

Gautam K, Hefzy MS, Mustapha AA, et al (2024) Comparison of opensim and anybody modeling systemtm predictions in biomechanical modeling of upper extremities. International Journal of Research in Orthopaedics 10(4):717

Gielen C, Houk JC (1984) Nonlinear viscosity of human wrist. Journal of Neurophysiology 52(3):553–569

Gojkovic Z, Ivancevic T, Jovanovic B (2019) Biomechanical model of swimming rehabilitation after hip and knee surgery. Journal of Biomechanics 94:165–169

Gonzalez D, Imbiriba LA, Jandre F (2025) Estimating continuous and intermittent feedback models of postural control using the least squares method. Biological Cybernetics 119(2):11

Gonzalez RC (2009) Digital image processing. Pearson education india

Goodfellow I (2016) Deep learning

Goodfellow I, Bengio Y, Courville A (2016) Deep Learning. MIT Press, http://www.deeplearningbook.org

Gračanin I, Djurović M, Stanić D, et al (2023) Prevention of shoulder injuries in swimmers. International Journal of Academic Health and Medical Research (IJAHMR) 7(2):186–190

Guignard B, Ayad O, Baillet H, et al (2021) Validity, reliability and accuracy of inertial measurement units (imus) to measure angles: application in swimming. Sports Biomechanics pp 1–33

Gull M, Bai S, Bak T (2020) A review on design of upper limb exoskeletons. Robotics 9:16

Gunawardane P, Pathirana A, Pallewela R, et al (2021) Additive gaussian noise model and kalman filter to enhance controllability of gesture-controlled teleoperated soft actuators. Proceedings of the Institution of Mechanical Engineers, Part B: Journal of Engineering Manufacture 235(14):2219–2229

Haghpanah SA, Khosrowpour E, Hematiyan MR (2023) An adaptive integral terminal sliding mode controller to track the human upper limb during front crawl swimming. European Journal of Sport Science 23(4):499–509

Hammond CV, Henninger HB, Fregly BJ, et al (2025) Personalization of closed-chain shoulder models yields high kinematic accuracy for multiple motions. Frontiers in Bioengineering and Biotechnology 13:1547373

Hou W, Wang P, Lv X, et al (2024) Swimming action recognition and analysis system based on intelligent algorithm. In: Proceedings of the First International Conference on Science, Engineering and Technology Practices for Sustainable Development, ICSETPSD 2023, 17th-18th November 2023, Coimbatore, Tamilnadu, India

Hu X, Dooley EA, Stefanyshyn DJ, et al (2025) An augmented full-body model that improves upper body tracking and reduces dynamic inconsistency in complex motion: X. hu et al. Annals of Biomedical Engineering pp 1–13

Huber ME, Folinus C, Hogan N (2019) Visual perception of joint stiffness from multijoint motion. Journal of neurophysiology 122(1):51–59

Ichikawa H, Ohgi Y, Miyaji C, et al (2003) Estimation of arm motion in front crawl swimming using accelerometer. Biomechanics and Medicine in Swimming IX, University of Saint-Etienne, France pp 133–138

Ichikawa H, Ohgi Y, Miyaji C, et al (2006) Estimation of arm joint angular displacements in front crawl swimming using accelerometer. Rev

Port Cienc 6:223–225

Iqbal K, Roy A (2004) Stabilizing pid controllers for a single-link biomechanical model with position, velocity, and force feedback. J Biomech Eng 126(6):838–843

Iqbal M, Rasool S (2025) Optimal position fuzzy control for coordinated movement of the ring and little fingers in an impaired human hand. Biological Cybernetics 119(4):24

Iqbal M, Jaffer M, Mahmood A (2013) Bond graph modeling with control synthesis of coordinated fingers movement. In: International conference on Modeling and Simulation, pp 25–27

James G, Witten D, Hastie T, et al (2023) Linear regression. In: An introduction to statistical learning: With applications in python. Springer, p 69–134

Jeon H, Lee D (2024) Bi-directional long short-term memory-based gait phase recognition method robust to directional variations in subject's gait progression using wearable inertial sensor. Sensors 24(4):1276

Jiang J, Yan K, Xia X, et al (2025) A survey of deep learning-based pedestrian trajectory prediction: Challenges and solutions. Sensors 25(3):957

Johnson JN, Gauvin J, Fredericson M (2003) Swimming biomechanics and injury prevention: new stroke techniques and medical considerations. The Physician and sportsmedicine 31(1):41–46

Johnson MA, Moradi MH (2005) PID control. Springer

Justus D, Brennan J, Bonner S, et al (2018) Predicting the computational cost of deep learning models. In: 2018 IEEE international conference on big data (Big Data), IEEE, pp 3873–3882

Lahmar O, Abdou L, Ghiloubi IB, et al (2025) Robustness analysis of lqr-pid controller based on pso and gwo for quadcopter attitude stabilization. Engineering Proceedings 87(1):105

Lauer J, Rouard AH, Vilas-Boas JP (2016) Upper limb joint forces and moments during underwater cyclical movements. Journal of biomechanics 49(14):3355–3361

Lecrivain G, Slaouti A, Payton C, et al (2008) Using reverse engineering and computational fluid dynamics to investigate a lower arm amputee swimmer's performance. Journal of Biomechanics 41(13):2855–2859

Li J, Qiu F, Gan L, et al (2024) Concurrent validity of inertial measurement units in range of motion measurements of upper extremity: A systematic review and meta-analysis. Wearable

Technologies 5:e11

Li L, Peng W, Chen J, et al (2025) Phase-specific biomechanical characterization of upper limb movements in stroke. Bioengineering 12(11):1144

Macaro A, Connick M, Beckman E, et al (2018) Using machine learning techniques and wearable inertial measurement units to predict front crawl elbow joint angle: a pilot study. ISBS Proceedings Archive 36(1):366

Marquina LZ (2025) Uses of artificial intelligence in personalizing sports training. Revista Tecnológica Ciencia y Educación Edwards Deming 9(2):70–95

Miniato MA, Anand P, Varacallo MA (2023) Anatomy, Shoulder and Upper Limb, Shoulder. StatPearls Publishing, Treasure Island (FL), [Updated 2023 Jul 24]. In: StatPearls [Internet]

Mononen ME, Turunen MJ, Stenroth L, et al (2024) Biomechanical modeling and imaging for knee osteoarthritis–is there a role for ai? Osteoarthritis Imaging 4(2):100182

Morais JE, Oliveira JP, Sampaio T, et al (2022) Wearables in swimming for real-time feedback: A systematic review. Sensors 22(10):3677

Morris KS, Jenkins DG, Osborne MA, et al (2019) The role of the upper and lower limbs in front crawl swimming: the thoughts and practices of expert high-performance swimming coaches. International Journal of Sports Science & Coaching 14(5):629–638

Nakashima M (2009) Modeling the dynamics of human swimming. Advances in Science and Technology 58:220–228

Oh S, et al (2025) Empowering artificial muscles with intelligence: recent advancements in materials, designs, and manufacturing. Materials Horizons 12(9):2764–2788

Okyere E, Bousbaine A, Poyi GT, et al (2019) Lqr controller design for quad-rotor helicopters. The Journal of Engineering 2019(17):4003–4007

O'sullivan P, Menolotto M, O'Flynn B, et al (2022) Estimation of maximum shoulder and elbow joint torques based on demographics and anthropometrics. In: 2022 44th Annual International Conference of the IEEE Engineering in Medicine & Biology Society (EMBC), IEEE, pp 4346–4349

Pennestri E, Stefanelli R, Valentini P, et al (2007) Virtual musculo-skeletal model for the biomechanical analysis of the upper limb. Journal of biomechanics 40(6):1350–1361

Pink MM, Tibone JE (2000) The painful shoulder in the swimming athlete. Orthopedic clinics of

north america 31(2):247–261

Poitras I, Bielmann M, Campeau-Lecours A, et al (2019) Validity of wearable sensors at the shoulder joint: Combining wireless electromyography sensors and inertial measurement units to perform physical workplace assessments. Sensors 19(8):1885

Prodanovic N, Dzunic D, Kocovic V, et al (2024) Application of the random forest algorithm for identifying abnormal patterns of knee joint movement. In: 2024 26th International Conference on Digital Signal Processing and its Applications (DSPA), pp 1–4

Riani A, Madani T, Benallegue A, et al (2018) Adaptive integral terminal sliding mode control for upper-limb rehabilitation exoskeleton. Control Engineering Practice 75:108–117

Rokach L, Maimon O (2005) Top-down induction of decision trees classifiers-a survey. IEEE Transactions on Systems, Man, and Cybernetics, Part C (Applications and Reviews) 35(4):476–487

Rubin RT, Lin S, Curtis A, et al (2013) Declines in swimming performance with age: a longitudinal study of masters swimming champions. Open Access Journal of Sports Medicine pp 63–70

Sabatini AM (2011) Estimating three-dimensional orientation of human body parts by inertial/magnetic sensing. Sensors 11(2):1489–1525

Saeed A, et al (2025a) Bond graph analysis of a three-link physiological motor control system: integrating simulation and muscle behavior. Biological Cybernetics 119(2):10

Saeed Z, Iqbal M, Imtiaz J (2025b) Biomechanical modeling and optimal control of a multi-joint human hand for precision motion. In: 2025 27th International Multitopic Conference (INMIC), IEEE, pp 1–6

Saraf P, Gupta M, Parimi AM (2020) A comparative study between a classical and optimal controller for a quadrotor. In: 2020 IEEE 17th India Council International Conference (INDICON), IEEE, pp 1–6

Sayahkarajy M, Witte H (2025) Empirical data-driven linear model of a swimming robot using the complex delay-embedding dmd technique. Biomimetics 10(1):60

Takagi H, Nakashima M, Sato Y, et al (2016) Numerical and experimental investigations of human swimming motions. Journal of sports sciences 34(16):1564–1580

Talamucci F (2024) Motion of general nonholonomic systems from the d'alembert principle via an algebraic method. Acta Mechanica pp 1–15

Van Crombrugge I, Sels S, Ribbens B, et al (2022) Accuracy assessment of joint angles estimated from 2d and 3d camera measurements. Sensors 22(5):1729

Vieira L, Costa MJ, Santos CC, et al (2024) Swimming velocity analysis using wearable inertial sensors and speedometer: A comparative study. Bioengineering 11(8):757

Von Loebbecke A, Mittal R, Gupta V, et al (2007) A comparative analysis of swimming styles in competitive swimming. In: APS Division of Fluid Dynamics Meeting Abstracts, pp EH–001

Voskakis D, Kelasidi E, Papandroulakis N (2024) Modeling and control of an underwater calibration arm. In: 2024 32nd Mediterranean Conference on Control and Automation (MED), IEEE, pp 81–87

Wang W, Lu Y (2018) Analysis of the mean absolute error (mae) and the root mean square error (rmse) in assessing rounding model. In: IOP conference series: materials science and engineering, IOP Publishing, p 012049

Wang Z (2024) Analysis of swimmers' technical movement optimization schemes using sports biomechanics algorithms. Journal of Electrical Systems 20(9s):1243–1253

Xingyu H, Zan M, Chao Y (2024) Image acquisition system based on optical sensors for swimmer technical analysis and simulation. Optical and Quantum Electronics 56(3):334

Xu Y, Hollerbach JM (1999) A robust ensemble data method for identification of human joint mechanical properties during movement. IEEE transactions on biomedical engineering 46(4):409–419

Yanai T, Hay JG, Miller GF (2000) Shoulder impingement in front-crawl swimming: I. a method to identify impingement. Medicine and science in sports and exercise 32(1):21–29

Zaidi H, Taiar R, Fohanno S, et al (2008) Analysis of the effect of swimmer's head position on swimming performance using computational fluid dynamics. Journal of Biomechanics 41(6):1350–1358

Zhang Z (2024) Quantum sensors in sports biomechanics in revolutionizing injury prevention. Optical and Quantum Electronics 56(3):311

Zhao F, et al (2024) The application of sports biomechanics in sports injury prevention and rehabilitation. Frontiers in Sport Research 6(3)

Supplementary Files

This is a list of supplementary files associated with this preprint. Click to download.

- datasettesting.csv
- DatasetTraining.csv